paths starting with widely different initial conditions. This strongly suggests that this state of motion is stable. Probably it is unique for ordinary launchings. It is plausible that each boomerang has a characteristic final state of motion. For instance, flight path calculations made for boomerang 195.1 (level 3) yielded a final state characterized by the values:

$$f = 9.2 \text{ rev/s, } V = 13.5 \text{ m/s, } U = 0.78, \ \dot{\Psi} = 9.2°, \ \vartheta = 61°, \ \psi = 161°,$$

$$\phi = 18.4 \ , \ \Delta Z = 22.1 \text{ m, } \Delta t = 4.7 \text{ sec.}$$

Necessary conditions for a boomerang's final state of motion are:

$$\dot{V} = 0, \ \dot{\omega}_z = 0, \ \ddot{\Psi} = 0, \ \dot{\vartheta} = 0, \ \dot{\psi} = 0. \tag{28.1}$$

These are 5 equations for the 5 unknowns V, ω_z, Ψ, ϑ, ψ. The equations can be solved by putting the right-handed sides of the equations (4.8) and (4.9) equal to zero. If (28.1) is satisfied, $\dot{\phi}$ = constant according to (4.9), and $\dot{Z}$ = constant while $\dot{X}$ and $\dot{Y}$ vary harmonically with ϕ according to (4.10). We shall not discuss the conditions for the existence, the stability, or the uniqueness of a boomerang's final state of motion.

In the boomerang flight presented in this section, the path curves counterclockwise (ϕ increases) until $t = 6.2$ sec. ($Z = 4.6$ m); after this ϕ decreases and the path curves clockwise. In other cases this reversal may occur at an earlier or at a later instant. This phenomenon can often be observed in real boomerang flights. Sometimes a boomerang may be well on its way to its final state of motion before it hits the ground. Curiously, the first counterclockwise loop, so characteristic for the flight of a right-handed boomerang, may be considered as merely a transient form of motion, soon leading up to the boomerang's final state.

In the final state of motion discussed above, the gravitational force plays a crucial role. What would happen in the absence of gravity? In the following we shall suppose that $g = 0$, that the air is homogeneous (with density $\mu = 1.20$ kg/m^3), and that there is no wind. The equations of motion (4.8), (4.9), (4.10) now are modified in an important aspect: for a given boomerang $\dot{V}$, $\dot{\omega}_z$ and $\ddot{\Psi}$ depend only on the aerodynamic forces, and hence (in our model) only on V, ω_z and Ψ. The shape of the boomerang's flight path is independent of ϑ_o, ϕ_o, ψ_o, X_o, Y_o, Z_o. The path in

(Ψ,U)-space traversed by the boomerang depends only on Ψ_o and U_o, while V_o (or f_o) determines the velocity at which this path is traversed.

A necessary condition for Ψ being stationary is given by (22.1), and for U being stationary by (22.2). The restriction $\vartheta = \frac{1}{2}\pi$, $\psi = 0$ is not relevant now because gravity is absent. The boomerang will travel to a point with $\dot{\Psi} = 0$, $\dot{U} = 0$: (Ψ^*,U^*) (under conditions not investigated by us). Because the boomerang continually loses kinetic energy V and ω_z (or f) decrease. Since $\dot{V}(:) - V^2$, V decreases inversely with time, and the boomerang's path length increases logarithmically with time. The boomerang ends up moving, slower and slower, along a helical path, away to infinity.

A gravitationless flight for boomerang 101.1 was computed with the initial conditions: $f_o = 10$ rev/s, $V_o = 25$ m/s, $\Psi_o = 0°$. This boomerang's final motion is characterized by:

$$\Psi^* = 2.0°, \quad U^* = 0.86$$

and the helical path by:

$$\emptyset = 34 \text{ m}, \quad \Delta R = 31 \text{ m}, \quad \Delta P = 112 \text{ m}, \quad \Delta n = 70$$

where $\emptyset$ is the diameter of the helix, ΔR is the difference in the boomerang's position, ΔP the path length and Δn the number of revolutions between two points one turn of the helix apart. The helix is traversed clockwise as seen from the point of launching. The direction of the helix' axis depends on ϑ_o, φ_o and ψ_o. The helical motion begins rather soon after the start: already at $t = 7$ sec. we have $\Psi = 2.0°$, $U = 0.86$. At $t = 18.3$ sec. the boomerang has completed 100 spin revolutions and $f = 2.9$ rev/s, $V = 4.7$ m/s. At $t = 94.1$ sec. 200 revolutions are completed and $f = 0.7$ rev/s, $V = 1.1$ m/s.

The relative simple shape of the flight path in the gravitationless case is due to the fact that the motion proceeds at constant values for Ψ and U. In the presence of gravity there is no fixed equilibrium point (Ψ^*,U^*), and the boomerang moves about in the (Ψ,U)-plane. Much of the charm of real boomerang flights originates from the interplay of aerodynamic and gravitational forces.

In the practice of boomerang throwing the influence of wind on the boomerang's flight can be an important factor. Even a very light breeze of 1 m/s may significantly alter the shape of a flight path. In the absence of wind it does not matter whether the boomerang is thrown to the south or to the north; the flight path will have the same shape. As soon as there is wind, the direction in which the boomerang is launched does matter, and the angle φ_o may be a very important parameter indeed. If the wind is too strong, a boomerang's performance may be spoilt, the boomerang is taken with the wind and invariably lands at a considerable distance downwind. On the other hand, a moderate breeze may assist a boomerang in coming back. After carrying out a few trial throws in which the angle φ_o is varied, the boomerang thrower may obtain perfect return flights. This is particularly pleasing if the boomerang in case is incapable of returning well under windless conditions. Usually the optimum launching conditions are such that $\beta - \varphi_o \approx 45°$ (β determines the wind's direction, see §8).

Two such cases are shown in fig. 29.1 and fig. 29.2. The 4 flight paths are computed for boomerang 245.1 (level 3), which is associated with boomerang L5, see §18. For the flights of fig. 29.1 the initial conditions are:

$f_o = 10$ rev/s, $V_o = 25$ m/s, $\Psi_o = 0$,

$\vartheta_o = 80°$, $\varphi_o = 0°$, $\psi_o = -20°$,

$X_o = 0$ m, $Y_o = 0$ m, $Z_o = 1.8$ m,

a) no wind,

b) $\beta = 45°$, $W_o = 1.3$ m/s, $W_1 = 0,6$ m/s/10 m.

In the flights of fig. 29.2 the initial conditions are the same, except that $\vartheta_o = 70°$, $\psi_o = -30°$.

	wind	t	P	n	D	Z_2	D_2	D_1	f_2	f_1	V'_1	Ψ'_2	U'_1
29.1	no	10.1	112.6	98.5	17.6	13.4	44.1	15.7	10.6	9.0	2.0	80.9	.10
	yes	9.9	121.9	94.6	1.2	15.9	41.1	0.9	10.3	8.9	2.9	80.1	.09
29.2	no	12.2	114.2	122.1	24.1	16.1	39.2	20.5	11.1	9.0	2.4	64.8	.11
	yes	13.3	122.0	134.0	4.3	18.0	34.0	2.6	11.3	9.0	2.1	52.8	.13

table 29.1. Some values for the flights of fig. 29.1 and 29.2.

fig. 29.1a

fig. 29.1b

245.1.

10	25	0
70	0	-30
0	0	1.8

fig. 29.2a

245.1

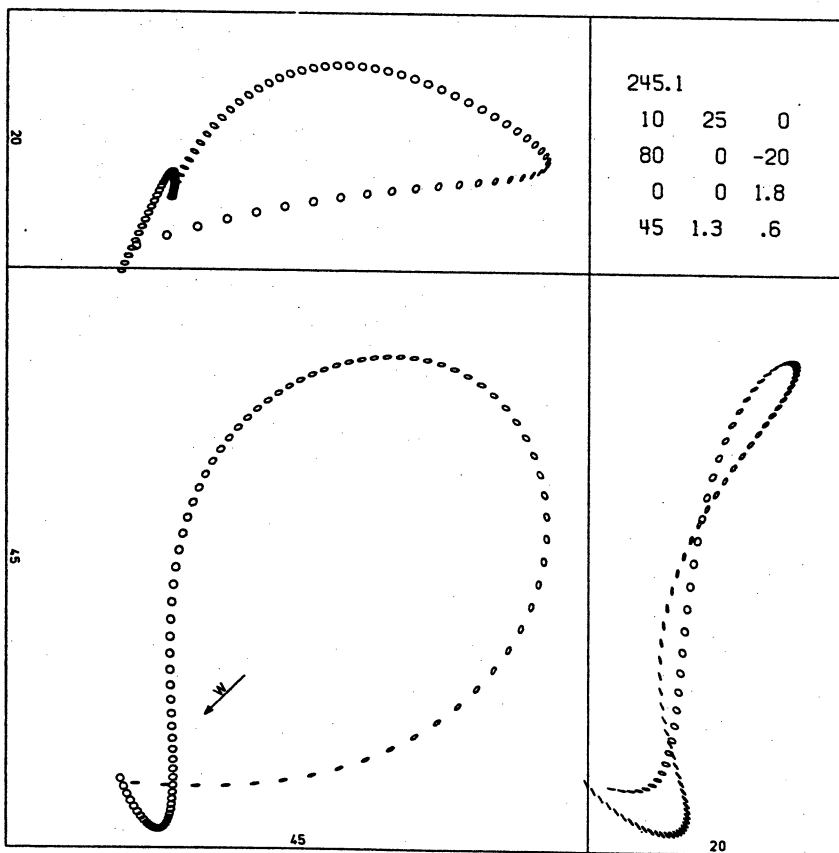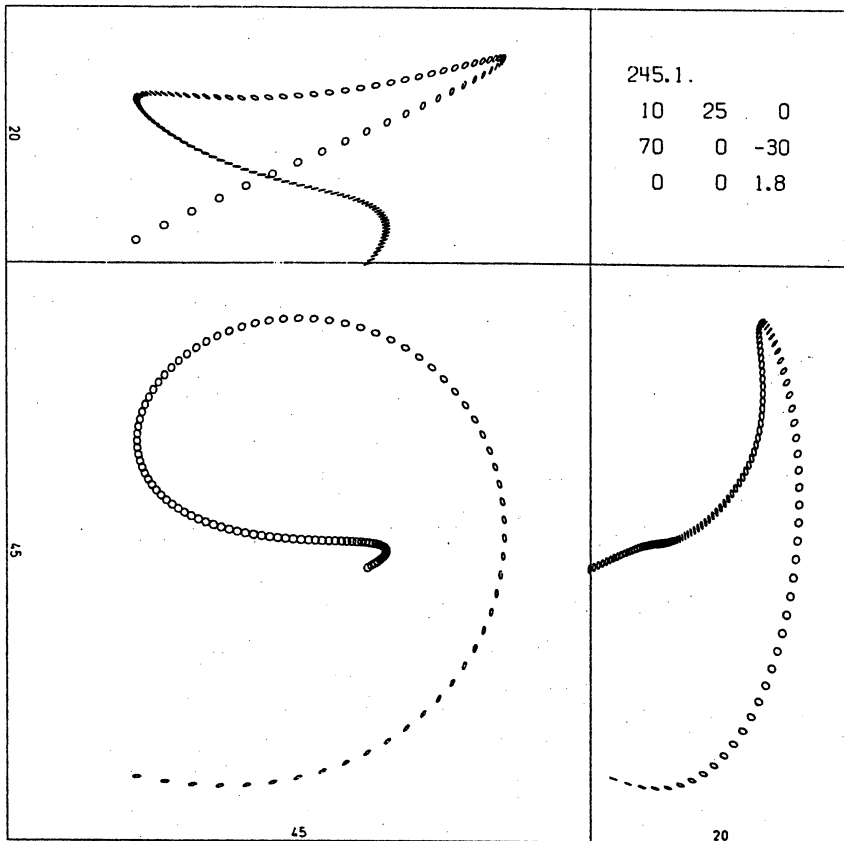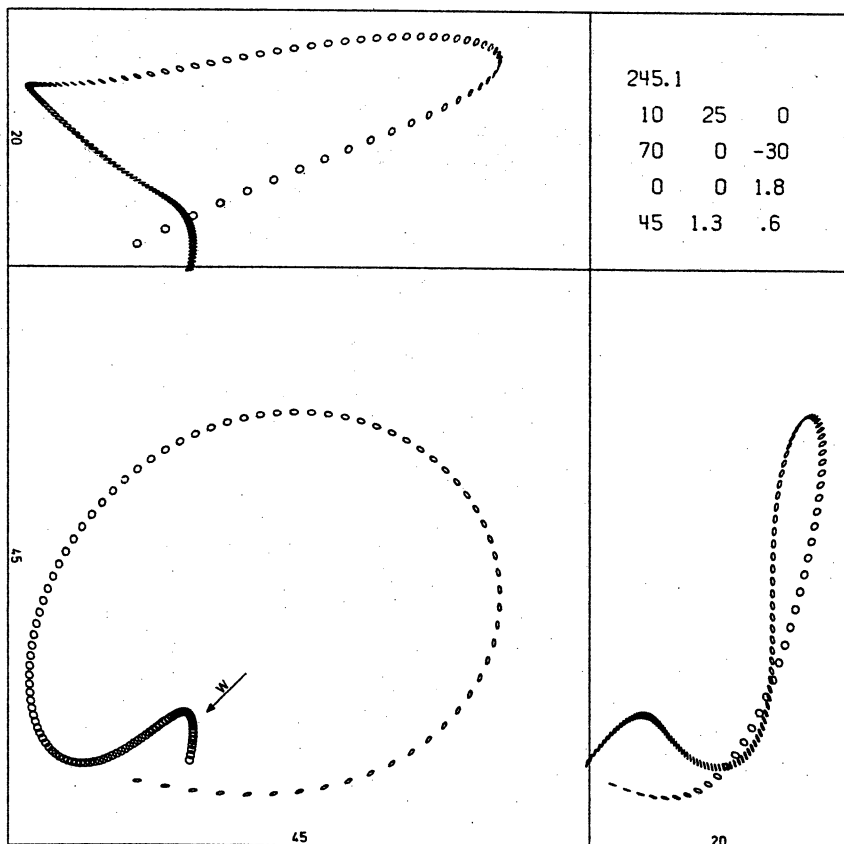| 10 | 25 | 0 |
70	0	-30
0	0	1.8
45	1.3	.6
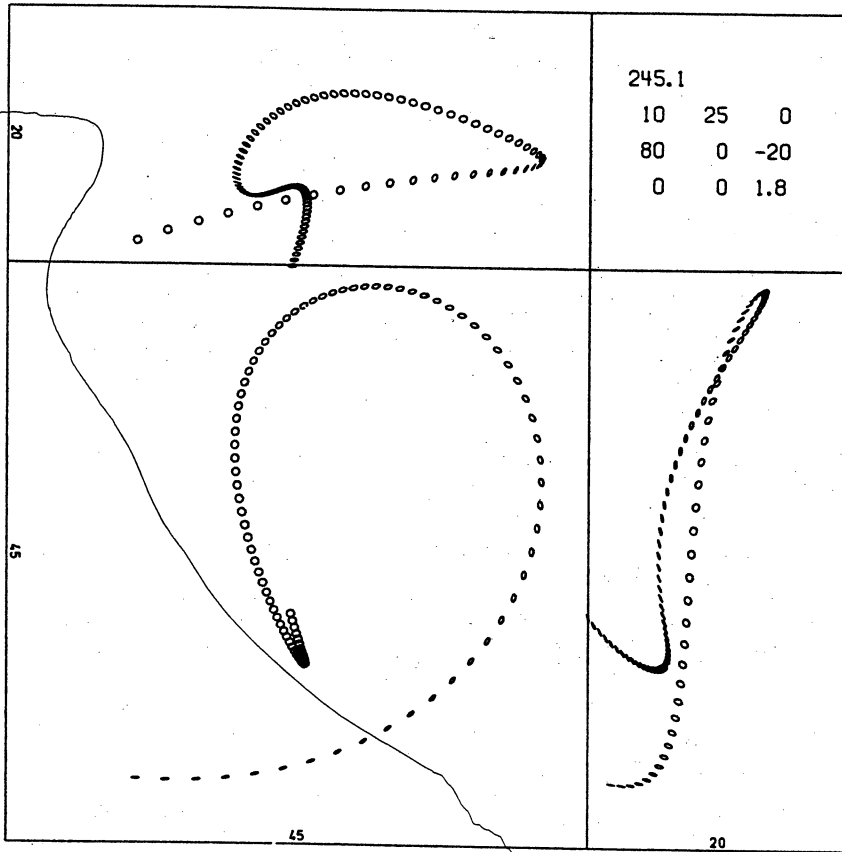
fig. 29.2b

Some values for these 4 flights are listed in table 29.1. In these examples the light breeze helps the boomerang to return beautifully. It is rather unfortunate that the field experiments with boomerang L5 (see §18) did not produce level 1 flight paths suitable for determining the influence of wind.

The main influence of the wind on a boomerang's flight can be explained as follows. Suppose the wind velocity field is constant and homogeneous ($W_1 = 0$). Use a coordinate system (X',Y',Z') moving with the air. In this inertial frame the air is motionless. However, the initial conditions for the boomerang's flight are modified: V_o, Ψ_o and U_o have to be replaced by V'_o, Ψ'_o and U'_o according to §8. For instance, if a boomerang is launched directly into the wind, $V'_o > V_o$ and $U'_o > U_o$. In the (X',Y',Z')-system the boomerang traverses an ordinary flight path, starting with the modified initial conditions. This trajectory can be transformed back to the old (X,Y,Z)-system according to:

$$
\left.
\begin{aligned}
X(t) &= X'(t) + tW\cos\beta \\
Y(t) &= Y'(t) + tW\sin\beta \\
Z(t) &= Z'(t)
\end{aligned}
\right\} \quad (29.1)
$$

where W is the constant wind speed. If W is very small, the modification of the initial conditions has little influence, and the main effect of the wind is that the velocity of the air is added to the velocity of the boomerang. If the flight lasts for a time T, the landing point is shifted downwind over a distance $\approx WT$. In reality the wind speed varies in space and time, but the above line of reasoning usually is qualitatively valid.

In fig. 29.3a through h flight paths are shown for boomerang 101.1 (level 2), which are computed with the initial conditions:
$f_o = 10$ rev/s, $V_o = 25$ m/s, $\Psi_o = 0°$,
$\vartheta_o = 80°$, $\varphi_o = 0°$, $\psi_o = -10°$,
$X_o = 0$ m, $Y_o = 0$ m, $Z_o = 1.8$ m,
$\beta = $ variable, $W_o = 2$ m/s, $W_1 = 1$ m/s/10 m.
The values chosen for β are respectively: $0°$, $45°$, $90°$, $135°$, $180°$, $225°$, $270°$, $315°$.

β	V'_o	U'_o	ψ'_o	D	Z_2
none	25.0	1.34	0.0	7.7	9.9
0°	27.1	1.45	0.0	27.1	13.0
45°	26.5	1.42	-3.3	20.0	12.6
90°	25.0	1.34	-4.9	14.6	10.6
135°	23.5	1.25	-3.7	17.9	8.2
180°	22.9	1.22·	0.0	22.1	6.8
225°	23.6	1.26	3.7	25.0	7.4
270°	25.2	1.34	4.9	28.1	9.4
315°	26.6	1.42	3.3	28.8	11.7

table 29.2. Some values for the flights of fig. 29.3.

The wind speed at ground level $Z = 0$ is 2 m/s, at $Z = 10$ m: 3 m/s and at the launching point: 2.18 m/s. Values for the "modified initial conditions", V'_o, U'_o, ψ'_o for these flights are listed in table 29.2 together with values for the maximum elevation Z_2 and the distance of the landing point D. In all 8 cases the average wind speed of about 2.5 m/s encountered by the boomerang spoils the return performance. Two main effects are visible: 1° the boomerang is transported downwind, and 2° the maximum height Z_2 increases with increasing values of cos $(\beta-\varphi)$, varying between 6.8 m for the throw downwind to 12.6 m for the throw upwind.
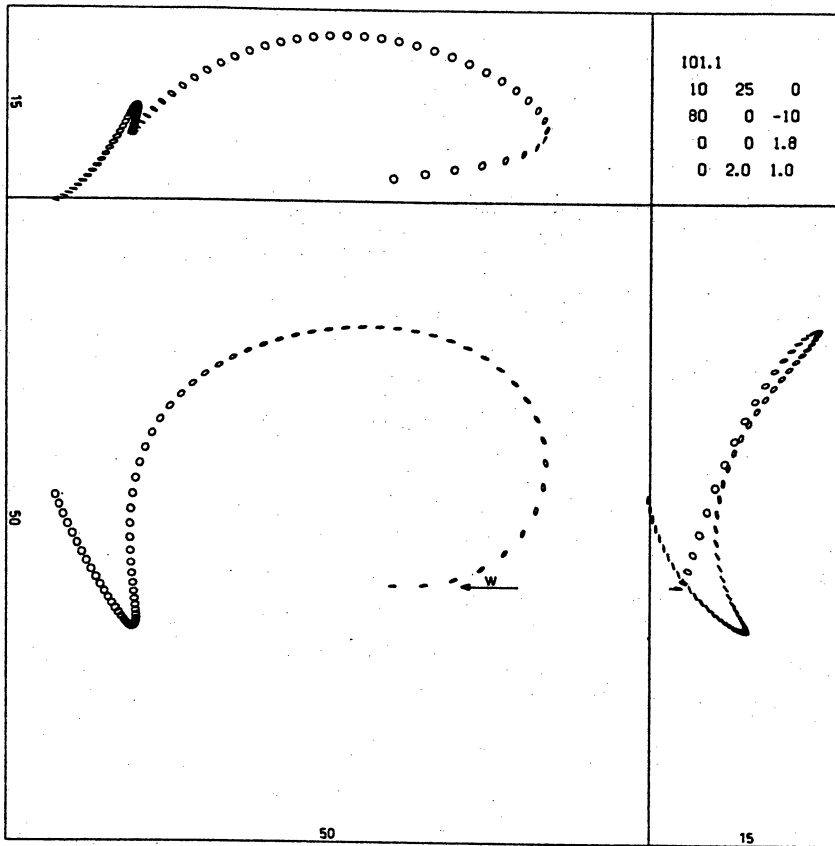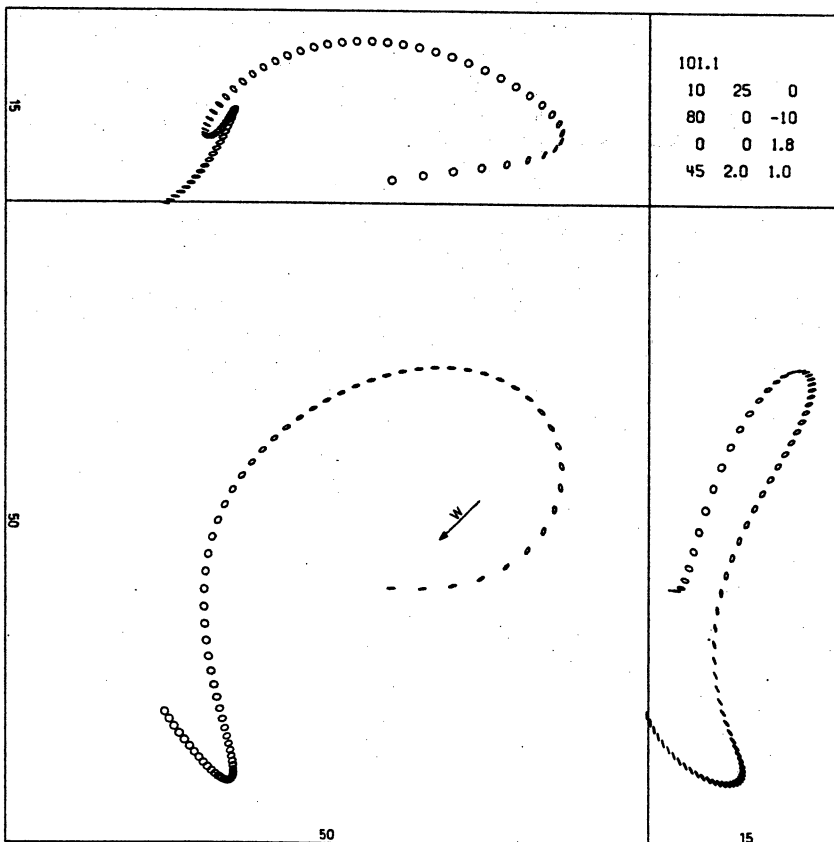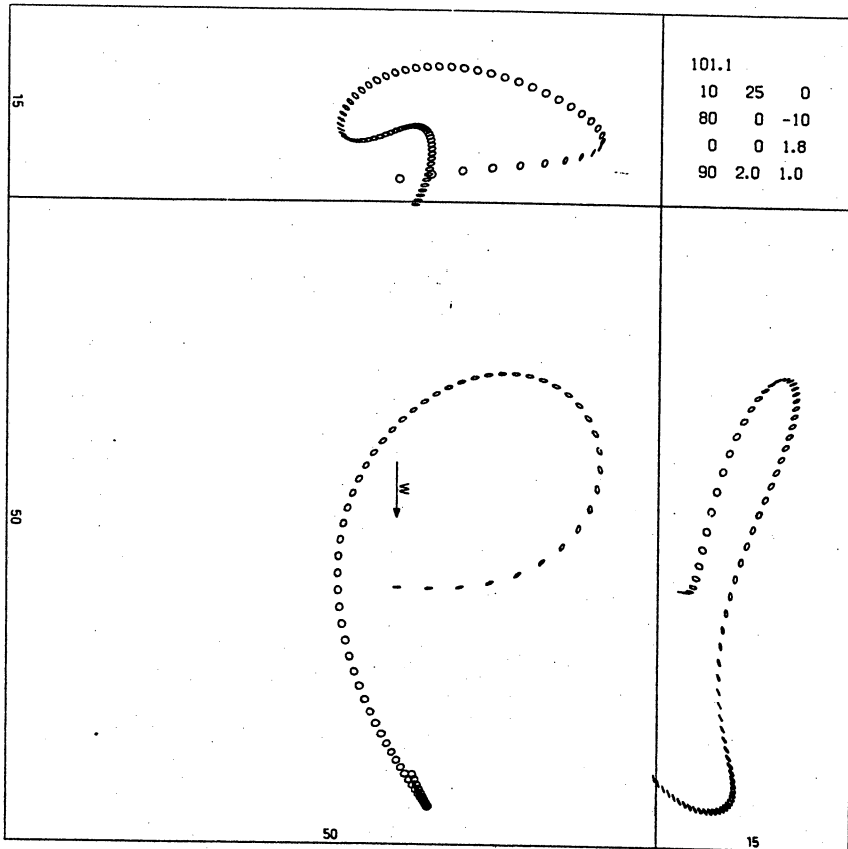
```
101.1
10   25    0
80    0  -10
 0    0  1.8
 0  2.0  1.0
```

fig. 29.3a


```
101.1
10   25    0
80    0  -10
 0    0  1.8
45  2.0  1.0
```

fig. 29.3b

515

fig. 29.3c

101.1
10	25	0
80	0	-10
0	0	1.8
90	2.0	1.0

fig. 29.3d

101.1
10	25	0
80	0	-10
0	0	1.8
135	2.0	1.0

101.1
10 25   0
80   0 -10
 0   0 1.8
180 2.0 1.0

w →

50

50   15   **fig. 29.3e**

101.1
10 25   0
80   0 -10
 0   0 1.8
225 2.0 1.0

w →

50

50   15   **fig. 29.3f**

101.1
10 25   0
80   0 -10
 0   0 1.8
270 2.0 1.0

fig. 29.3g

101.1
10 25   0
80   0 -10
 0   0 1.8
315 2.0 1.0
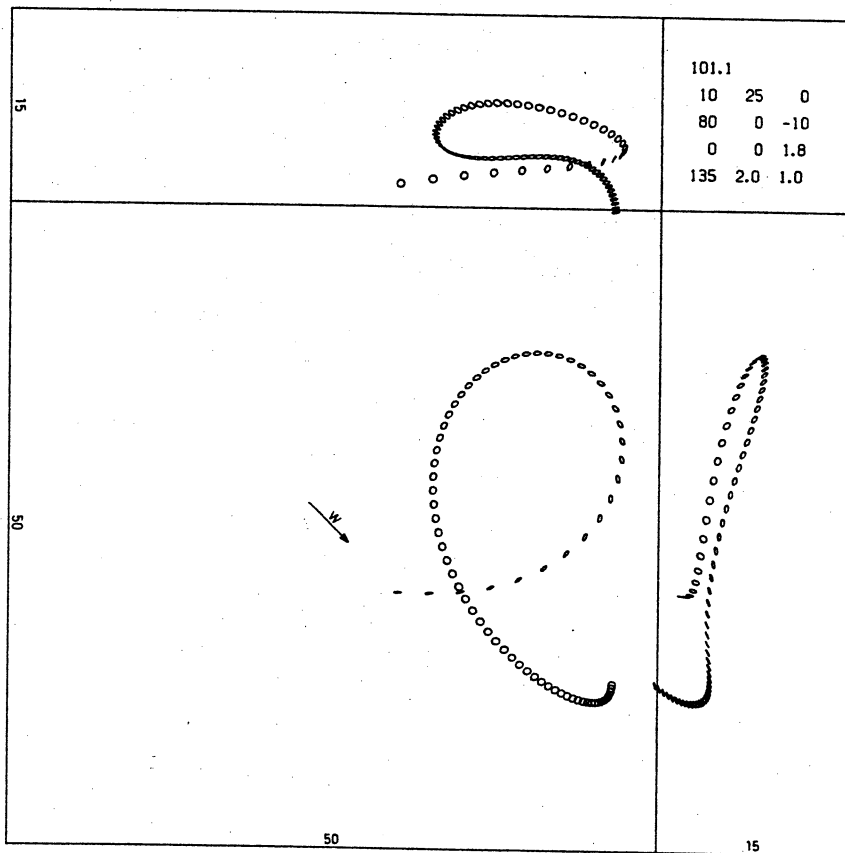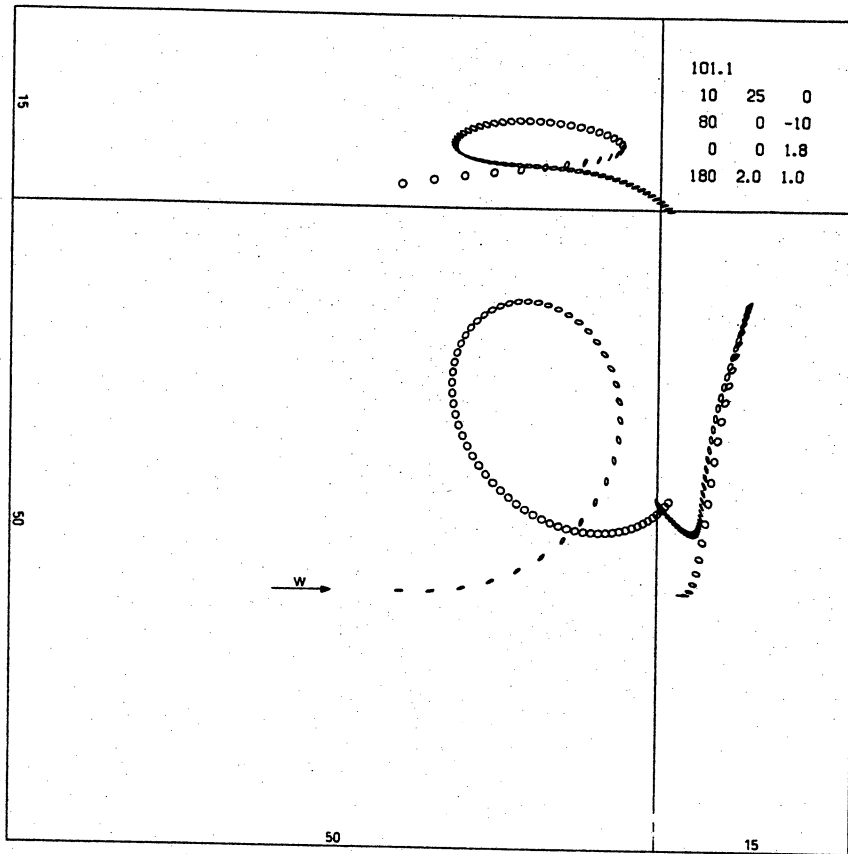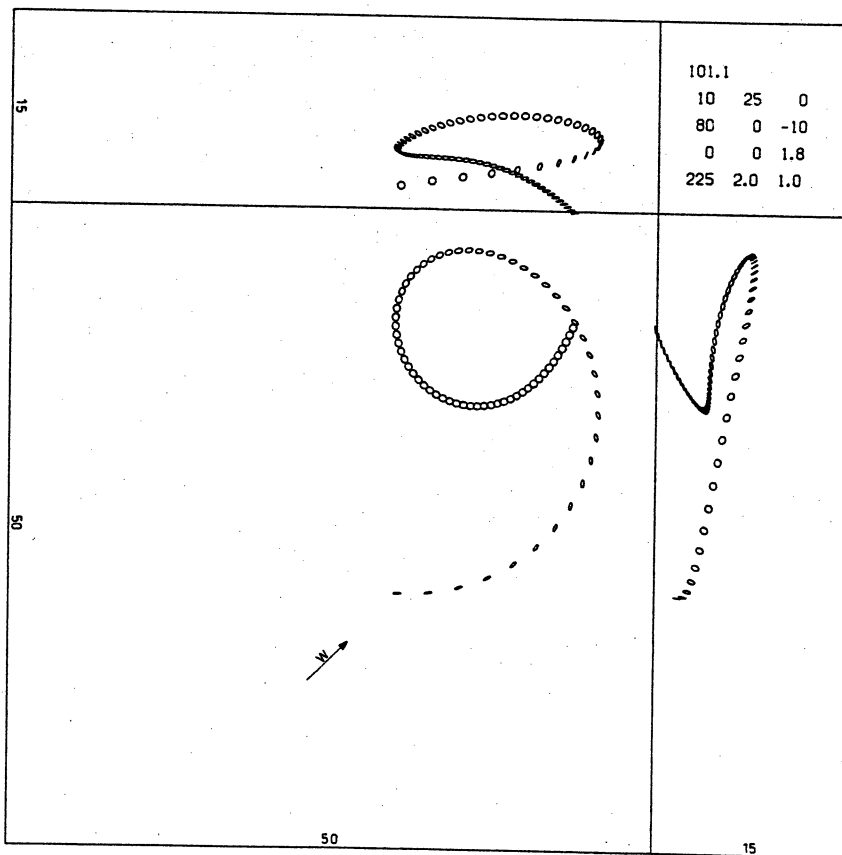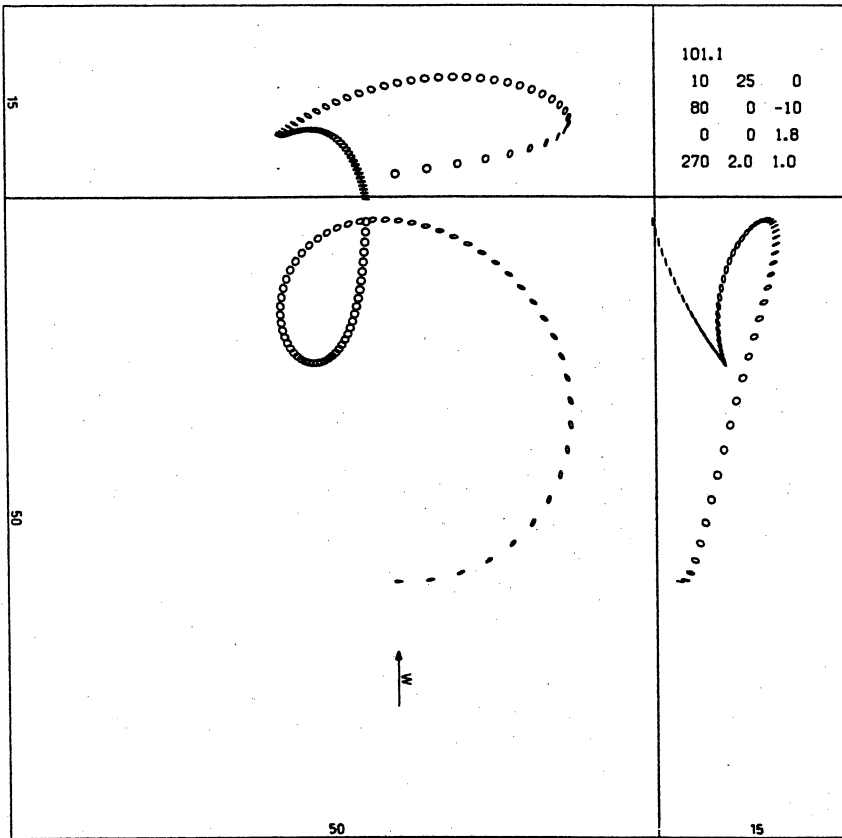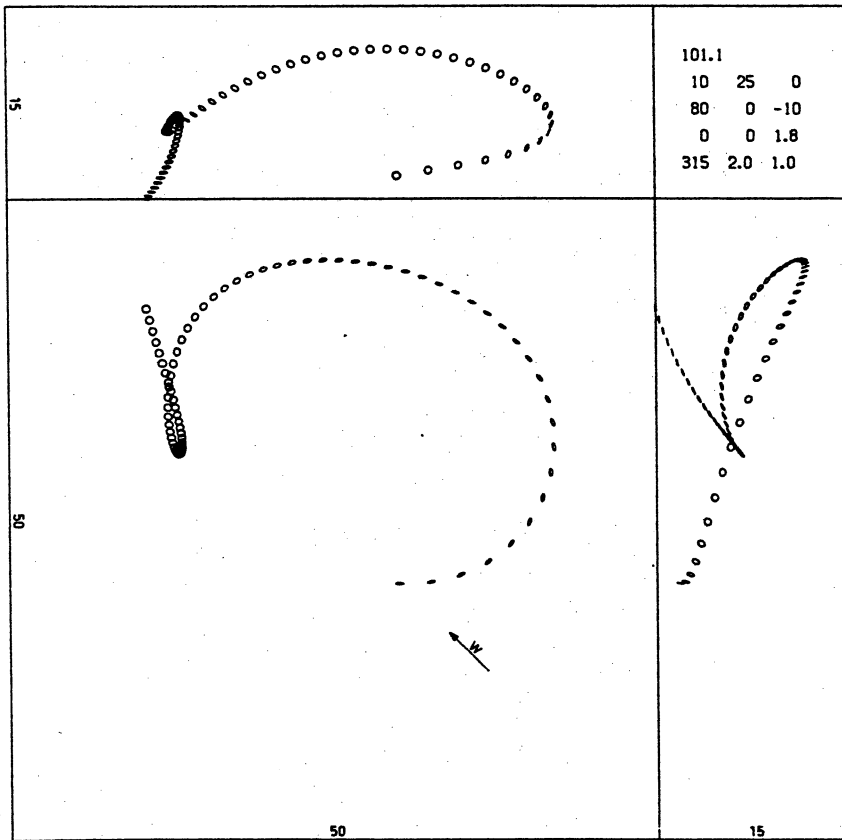
fig. 29.3h

Two experimental examples showing the influence of a change in a boom-
erang's mass distribution on the diameter of the flight path are given
in fig. 30.1 and fig. 30.2. These contain level 1 flight path stereo-
grams for boomerang L1 plain and boomerang L1 weighted.

|	a (m)	m (kg)	I_3 (kg. m^2)	λ
L1 plain	.298	.173	.00396	.258
L1 weighted	.298	.188	.00455	.272
difference	0	9%	15%	5.5%

Table 30.1. Mass distribution for L1 plain and L1 weighted. $\lambda = I_3/ma^2$.

The stereograms of fig. 30.1 are roughly similar in shape, they indicate
a flight path diameter of about 22 m for the L1 plain, and about 28 m
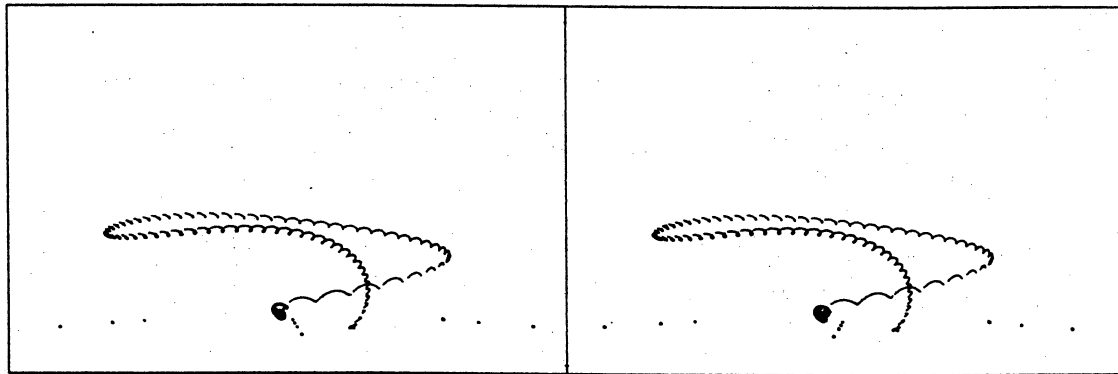for the L1 weighted.

To investigate the influence of m and I_3 on boomerang flights, a number
of model boomerangs were used, based on boomerang 101.1 (level 2), but
with different values for m and I_3. They are listed in tabel 30.2.
Boomerang 101.6 is almost identical with boomerang 101.1, the other six
boomerangs differ by a factor 2 either in m or in I_3 or in both.

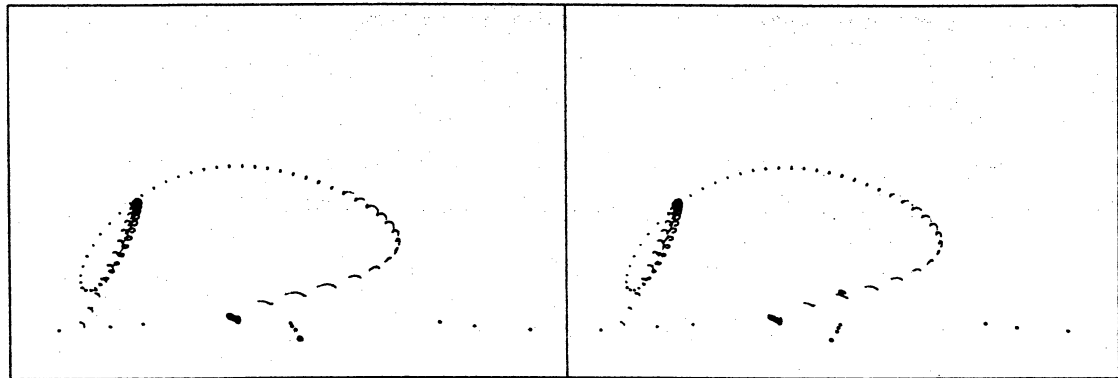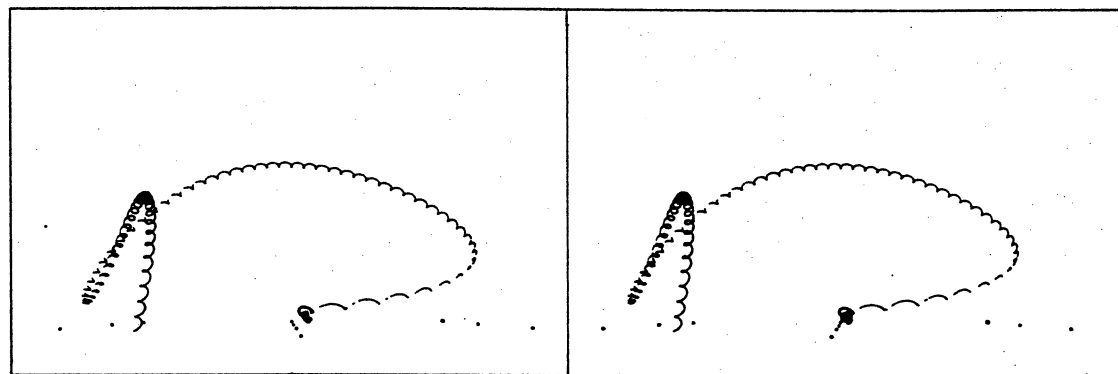| boomerang nr.	m (kg)	I_3 (kg. m^2)	λ
101.3	.080	.0020	.282
101.4	.160	.0020	.141
101.5	.080	.0040	.564
101.6	.160	.0040	.282
101.7	.320	.0040	.141
101.8	.160	.0080	.564
101.9	.320	.0080	.282

Table 30.2. Mass distributions for the 7 model boomerangs.
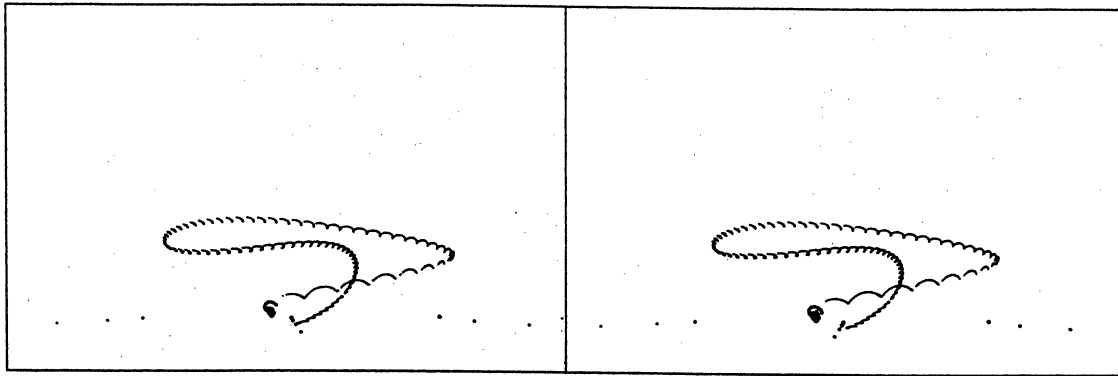
fig. 30.1. a: Ll plain, {1}, 7R6/L6A. b: Ll weighted, {1}, 11R19A/L19.

fig. 30.2. a: Ll plain, {1}, 4R8/L7A. b: Ll weighted, {2}, 11R9A/11L9.

Figure 30.1a through h shows 8 flight paths computed for these boomerangs. In 7 of these the initial conditions are:

$f_o = 10$ rev/s, $V_o = 25$ m/s, $\Psi_o = 0°$,

$\vartheta_o = 80°$, $\varphi_o = 0°$, $\psi_o = -10°$,

$X_o = 0$ m, $Y_o = 0$ m, $Z_o = 1.8$ m,

no wind.

The additional flight for boomerang 101.9 has the same initial conditions, except that $f_o = 12$ rev/s, $V_o = 30$ m/s.

bnr	t	P	n	D	Z_2	D_2	D_1	f_2	f_1	V_1	Ψ_2	U_1
101.3	8.4	66.9	56.4	3.6	9.6	11.6	1.3	10.0	5.9	2.1	24.2	.19
101.4	2.8	32.4	29.5	9.0	7.8	10.2	9.1	12.7	8.7	7.3	25.2	.34
101.5	7.7	85.1	49.8	21.9	3.5	33.5	19.0	10.0	5.5	4.0	20.2	.38
101.6	8.3	81.6	72.6	11.6	9.8	23.4	2.4	10.0	8.2	3.2	33.8	.20
101.7	3.2	41.1	37.6	17.6	7.1	21.5	17.6	12.7	9.9	7.4	28.1	.31
101.8	1.7	37.1	15.6	34.7	3.1	34.7	-	10.0	8.5	20.3	0.6	1.25
101.9	5.7	84.7	59.1	30.7	5.8	43.4	30.7	10.9	9.6	8.7	16.9	.43
101.9	9.2	125.9	106.9	12.0	11.5	45.6	10.4	12.2	11.3	4.2	45.0	.18

Table 30.3. Some values for the flights of fig. 30.1. Last row: $f_o = 12$, $V_o = 30$. Flight of 101.5 has minimum $\Psi = -1.2°$. Flight of 101.8 has minimum $\Psi = -0.7°$, D is increasing as the 101.8 reaches $Z = 0$.

Some values for the 8 flights of fig. 30.1 are listed in table 30.3. The relatively large differences in m and/or I_3 obviously give rise to dramatic differences in the shape of the flight paths. Boomerangs with equal values for λ have more or less similarly shaped flight paths which differ primarily in size. This rough similarity can also be observed in table 30.4, which lists some values of the flights at the instant at which $\dot\Psi = 0$ occurs for the first time. It is evident that boomerangs with low λ reach high values of Ψ and reversely. Again this phenomenon can be explained on the basis of the exposition given in the second half of §22.

In §7 it was shown that boomerangs such as 101.3, 101.6 and 101.9, which differ only in average density, but have the same λ, can traverse exactly similar flight paths, provided they are launched at the appropriate

bnr	t	f	V	U	Ψ
101.3	0.3	9.5	21.2	1.20	6.9
101.4	0.5	11.9	14.6	0.65	24.2
101.5	0.6	8.8	20.1	1.22	-1.2
101.6	0.8	9.5	19.4	1.09	7.8
101.7	1.0	11.9	13.6	0.61	28.1
101.8	0.5	9.5	22.6	1.27	-0.7
101.9	not	reached			

Table 30.4. First instant t at which $\dot{\Psi}$ = 0 occurs, and values of f, V, U, Ψ at that instant.

speed and spin. Suppose that, in accordance with table 7.1, row 3, we launch the three boomerangs with values for f_0 and V_0 as listed in table 30.5. Then we know that the flight path diameter for boomerang 101.3 is half that for boomerang 101.6, and that the flight path diameter of boomerang 101.9 is twice that for boomerang 101.6. The corresponding values for D_2 are listed in table 30.5. It is interesting to note that these values do not deviate much from those listed in table 30.3. This again shows that the flight path diameter is not very sensitive to the speed at which a boomerang is launched (provided that U_0 is constant, see §26).

bnr	f_0	V_0	D_2
101.3	7.1	17.7	11.7
101.6	10.0	25.0	23.4
101.9	14.1	35.4	46.8

Table 30.5. Some values for similar flight paths.

It may be interesting to note the influence of the insertion of batteries in the elbow of an experimental boomerang. This increases m, but hardly I_3 (see §10). The addition of the batteries' mass causes the boomerang's angle of incidence to increase, which decreases the resulting flight path diameter. To a somewhat exaggerated degree this effect can be seen by comparing the computed flights for boomerangs 101.3 and 101.4 in fig. 30.3a and b, or the flights for boomerangs 101.5, 101.6 and 101.7 in fig. 30.3c,d and e.
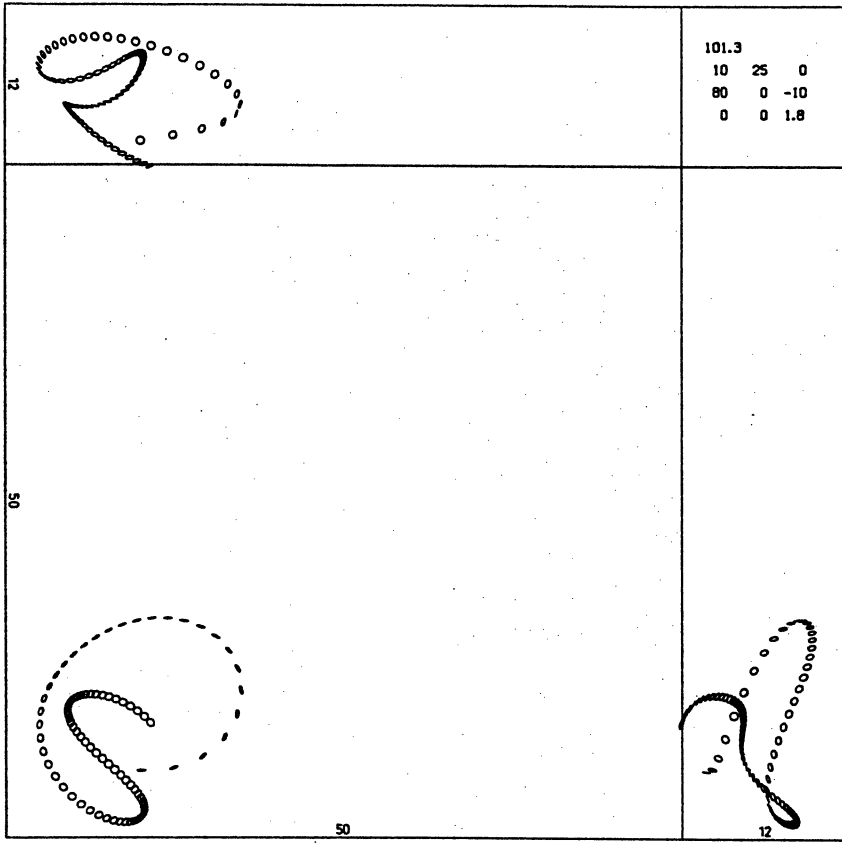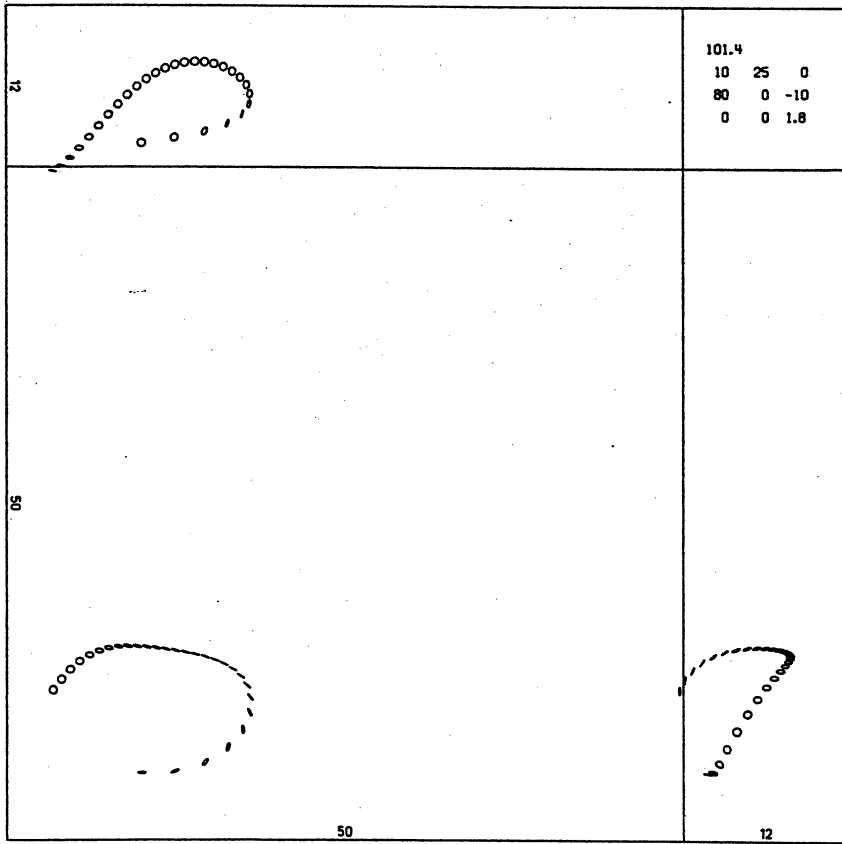
101.3
10 25   0
80   0 -10
 0   0 1.8

12

50

50

12

fig. 30.3a

101.4
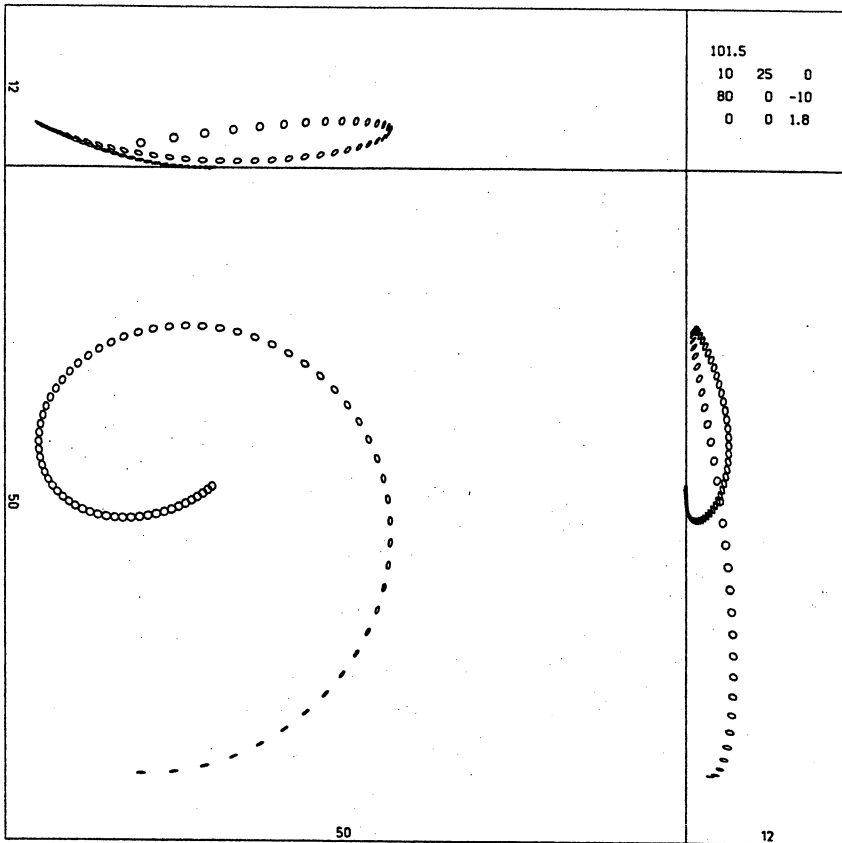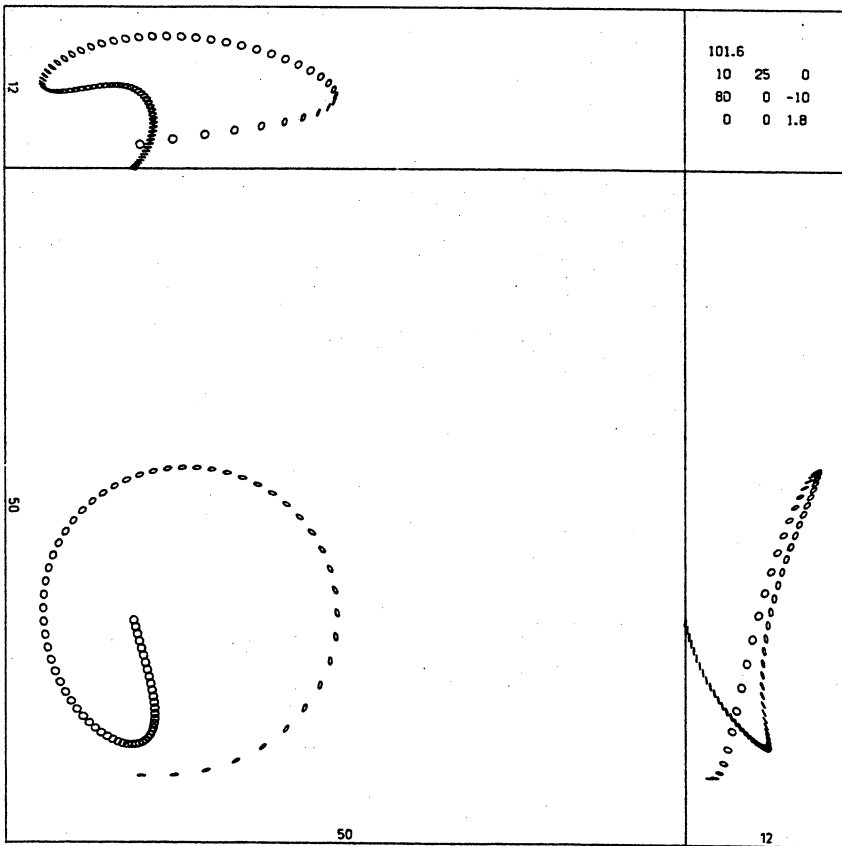10 25   0
80   0 -10
 0   0 1.8

12

50

50

12

fig. 30.3b

523

fig. 30.3c

fig. 30.3d

fig. 30.3e

fig. 30.3f

525

fig. 30.3g

fig. 30.3h

526
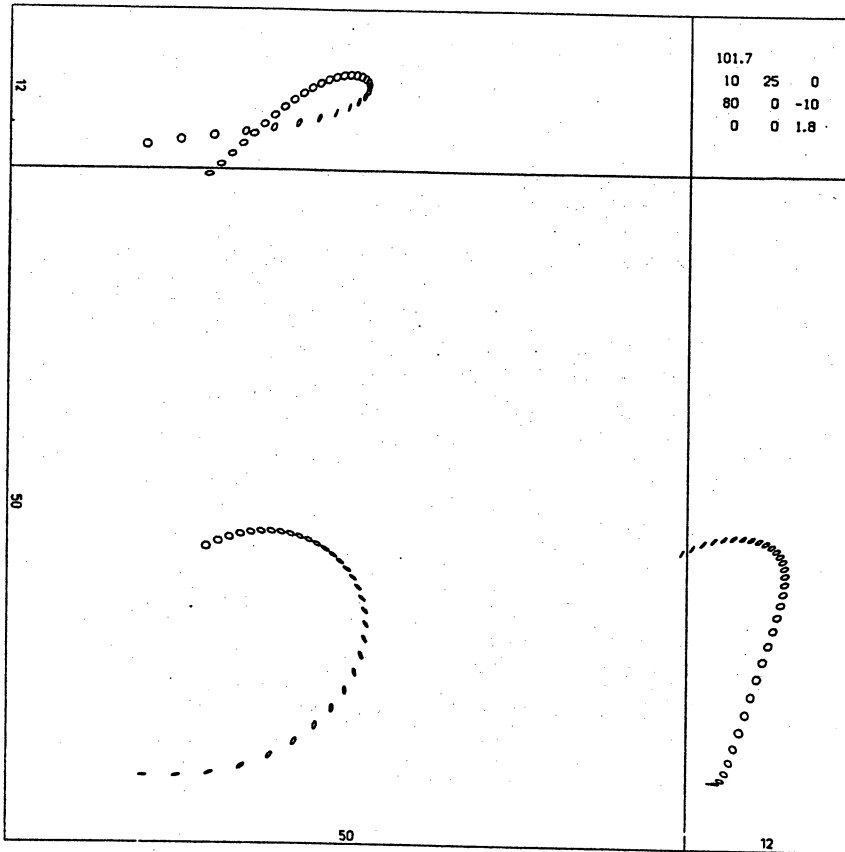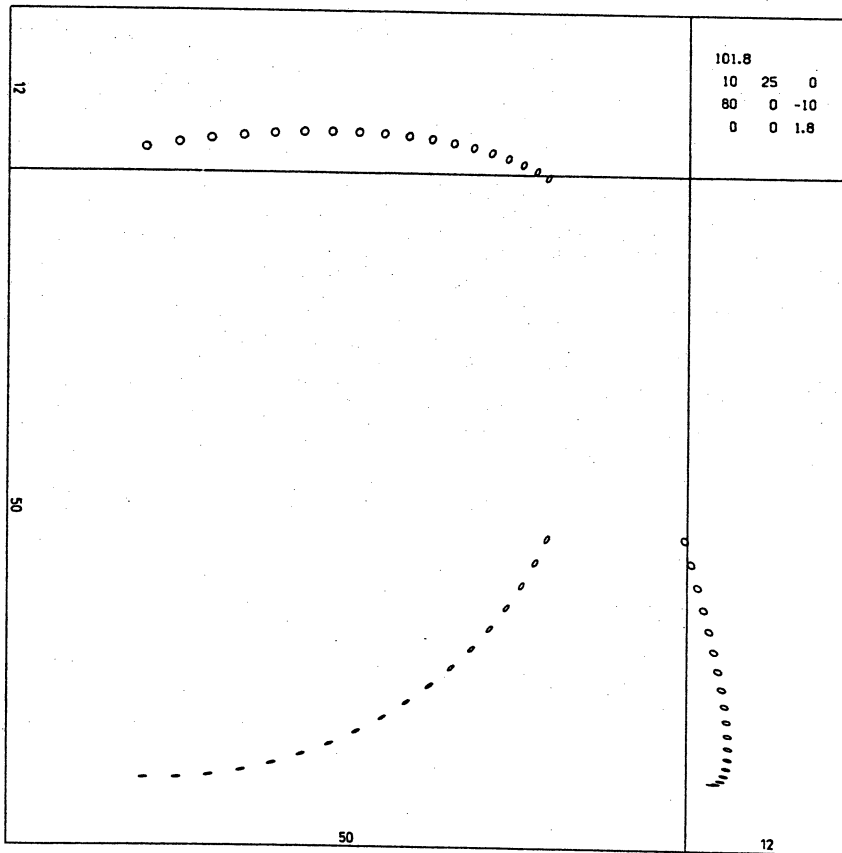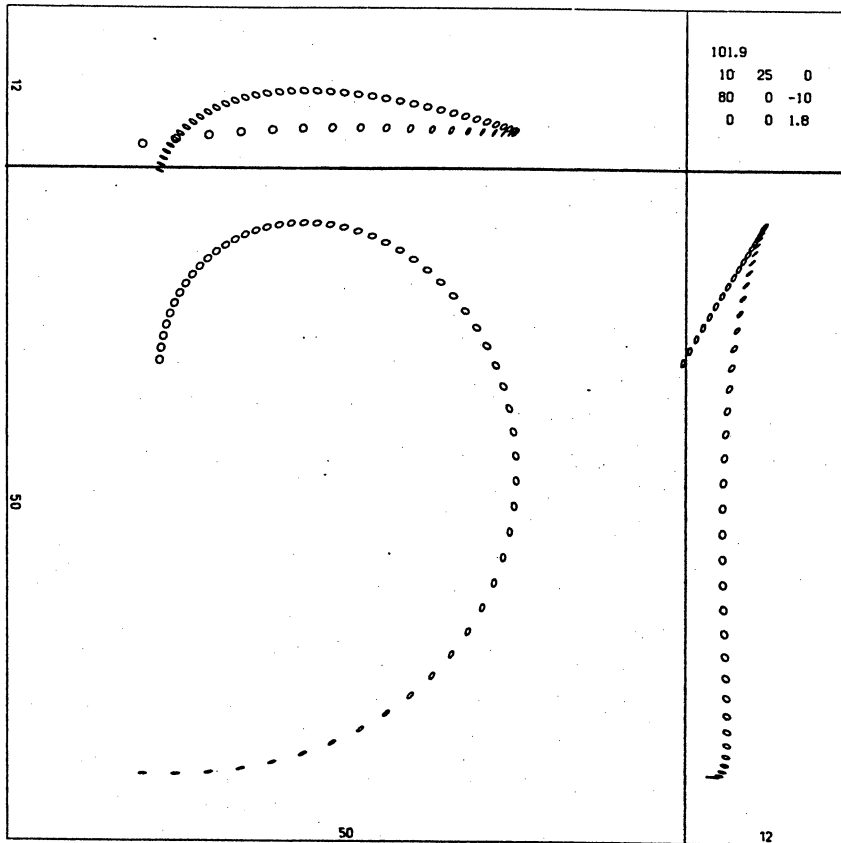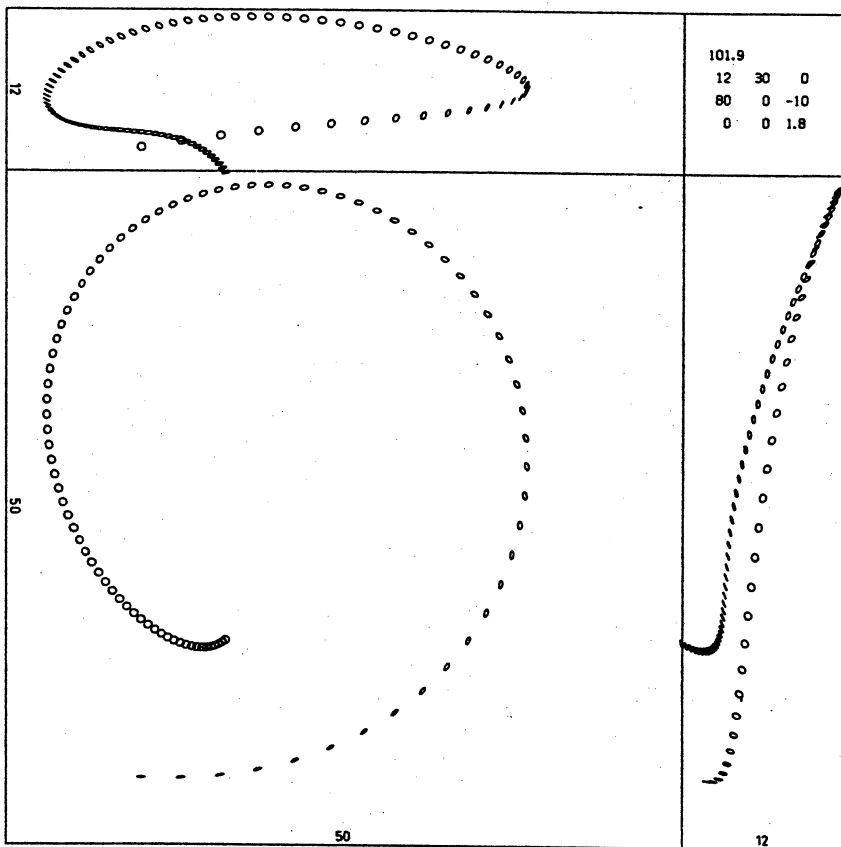
C_{L2} is the maximum lift coefficient for a boomerang arm's profile. In Part II, §22 the parameters characterizing the aerodynamic properties of level 3 model boomerangs are defined (see especially Part II, fig. 22.1). For moderate angles of incidence α^* ($\alpha_1 \leq \alpha^* \leq \alpha_2$) the profile lift coefficient C_L varies linearly with α^*. At $\alpha^* = \alpha_2$ C_L reaches its maximum value C_{L2}. For higher values of α^* stall occurs, and C_L decreases below C_{L2}.

The wind tunnel experiments reported in Part II, §26 indicated a value for C_{L2} of about 1.2 at most. The measurements were done on boomerang arms put in a straight airflow. In Part II, §32 it was shown that such low values of C_{L2} are unrealistic for boomerang arms forming part of *rotating* boomerangs. One of the reasons for including the present section is that it shows how poor the flight performance is of model boomerangs having arms with C_{L2} = 1.2.

boomerang nr.	normal profile C_{L2}	reversed profile C_{L2}
222.1	1.2	1.2
217.1	1.6	2.4
195.1	2.0	2.4
260.1	4.0	4.0

Table 31.1. C_{L2} values of model boomerangs.

Figure 31.1a through d shows 4 flight paths traversed by boomerangs differing only in C_{L2} and being otherwise identical with level 3 boomerang 195.1 (which is associated with boomerang L1 plain), see Part II, table 32.1. Table 31.1 lists the C_{L2} values for these boomerangs. The initial conditions in all 4 cases are:

f_o = 11 rev/s, V_o = 27 m/s, Ψ_o = 0°,

ϑ_o = 90°, φ_o = 0°, ψ_o = -20°,

X_o = 0 m, Y_o = 0 m, Z_o = 1.8 m,

no wind.

222.1

11	27	0
90	0	-20
0	0	1.8

fig. 31.1a

217.1

11	27	0
90	0	-20
0	0	1.8

fig. 31.1b

195.1

11	27	0
90	0	-20
0	0	1.8

fig. 31.1c

260.1

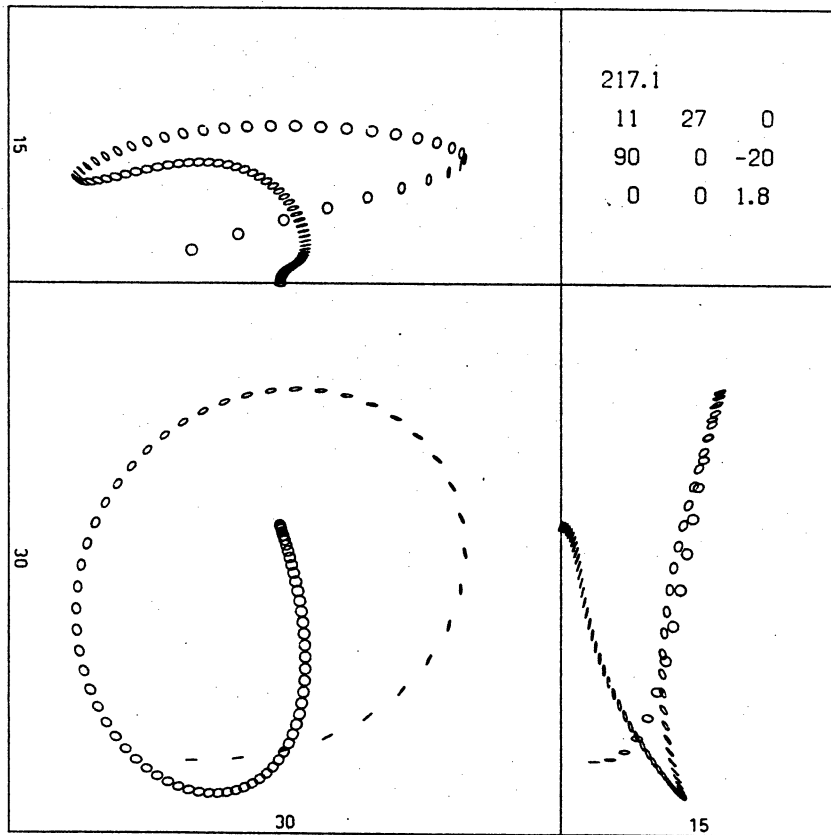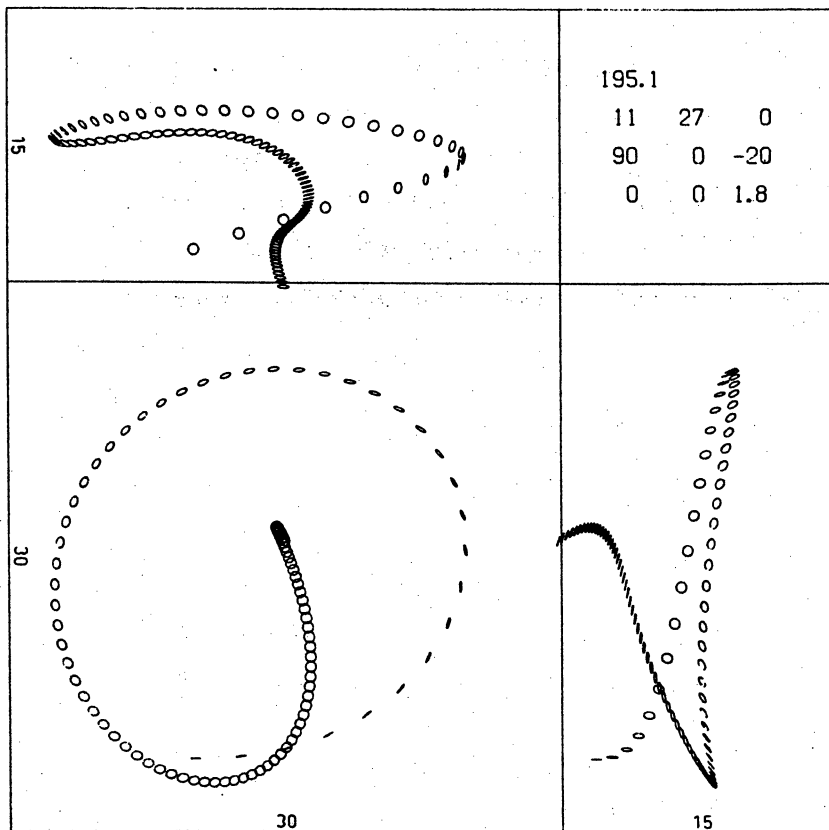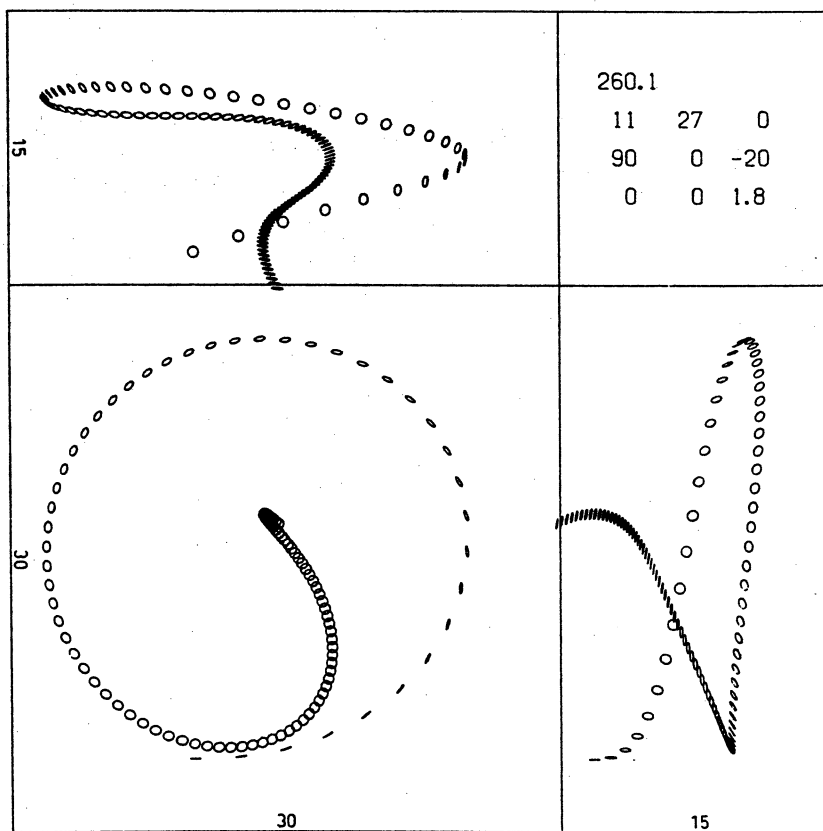| 11	27	0
90	0	-20
0	0	1.8
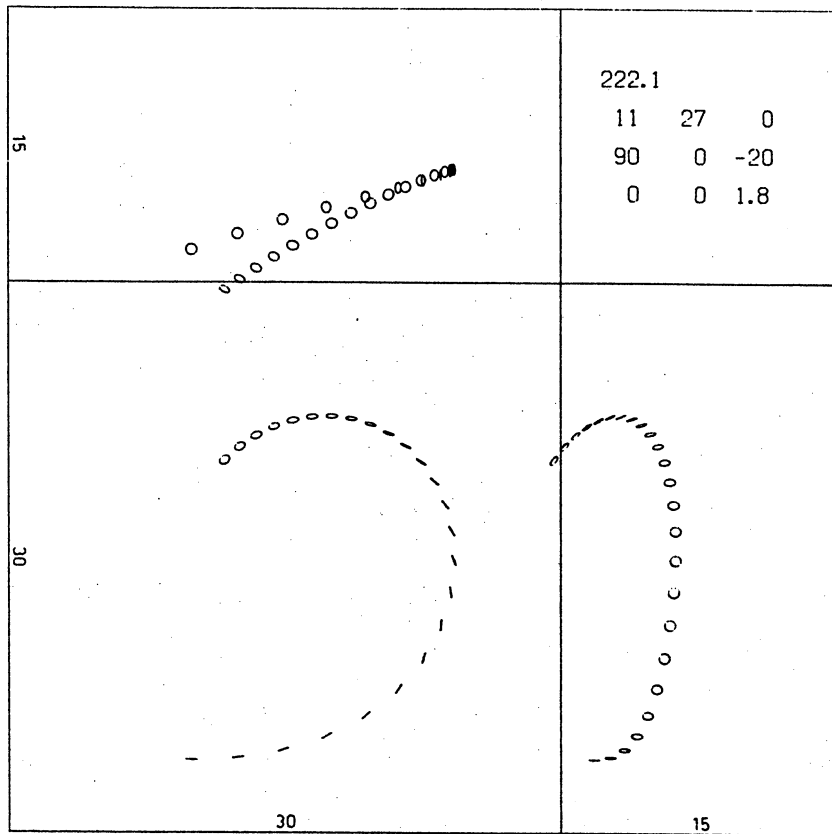
fig. 31.1d

Fig. 31.1a clearly indicates that boomerang 222.1 is a very poor boomerang indeed. The three other boomerangs all perform satisfactory return flights. In tables 31.2 and 31.3 some values for the flights are listed. The 4 flight paths differ significantly in maximum elevation (Z_2), which increases with increasing C_{L2}. Table 31.3 gives values of f,V,U and Ψ at t = 1.1 sec. (Approximately at this instant $\dot\Psi$ = 0 occurs for the first time in each of the flights.) We see: the lower C_{L2}, the stronger the initial decrease of V, and the higher the resulting value of Ψ.

bnr	t	P	n	D	Z_2	D_2	D_1	f_2	f_1	V_1	Ψ_2	U_1
222.1	2.4	39.8	24.5	16.4	6.2	20.7	16.4	11.0	9.9	11.9	21.3	.64
217.1	8.7	87.4	84.8	13.7	8.2	21.7	1.6	11.0	9.3	1.5	88.0	.08
195.1	10.2	92.3	99.1	12.9	9.4	22.3	1.2	11.0	9.4	1.7	85.7	.09
260.1	11.0	96.5	104.5	13.7	10.8	23.7	0.8	11.0	8.5	2.2	83.7	.13

Table 31.2. Some values for the flights of fig. 31.1.

bnr	t sec	f rev/s	V m/s	U	Ψ degr
all	0	11.0	27.0	1.31	0.0
222.1	1.1	10.2	14.4	0.76	20.9
217.1	1.1	10.3	17.8	0.92	12.9
195.1	1.1	10.3	18.3	0.93	10.9
260.1	1.1	10.2	19.0	1.00	8.7

Table 31.3. Some values for the flights after 1.1 sec.

According to Part. II, §22, the width of a model boomerang arm is
determined by giving the chord length c_t at the tip and c_r at the
root of the arm. In this section we consider three boomerangs having
arms with constant chord, i.e. with $c_t = c_r$. These boomerangs differ
from each other in chord, but their other aerodynamic parameters are
identical with those of level 3 boomerang 239.1 (which is associated
with boomerang WU), see Part II, table 32.1. Values for the chord
lengths and for the mass distributions of the boomerangs to be
compared are listed in table 32.1

boomerang nr	chord arm 1 (m)	chord arm 2 (m)	m (kg)	I_3 (kg.m^2)
244.2	.020	.020	.080	.0228
239.1	.040	.039	.160	.0456
267.3	.060	.060	.240	.0684

Table 32.1. Parameters in which the 3 boomerangs differ (a = .296 m).

The chords of the three boomerangs are in the proportion 1:2:3 (with
a slight deviation for arm nr. 2 of boomerang 239.1). The values for
m and I_3 are based on those for boomerang 239.1 and are chosen in the
same proportion 1:2:3. Why are m and I_3 chosen this way? The differences
in chord lead to corresponding differences in the aerodynamic forces.
These in turn would lead to predictable differences in the flight paths
if m and I_3 would be constant: the boomerang with the broadest arms
would have the smallest flight path diameter. On the other hand, if
the three boomerangs would have similar profiles, and be made of the
same material, the masses would be in the proportion 1:4:9. The
influence of mass would now be predominant, and the boomerang with
the broadest arms would have the largest flight path diameter.

In the following discussion we refer to the winglet model described
in Part II, §2. If the chords of the boomerang arms are multiplied
by a constant factor f, the winglets' density in the circular region

S is multiplied by f also. As long as the winglets' density is very small, the lift distribution on the winglet system (at given V, ω_z, Ψ) changes by the same factor f. At higher densities, however, the lift distribution does not change proportionally, but, for instance, the peak at the leading edge of S grows relatively stronger. (The theoretical background is discussed in Part II, §4.) This leads us to expect that the ratio T_{1y}/F_{1z} increases with increasing chord lengths. This is indeed confirmed by table 32.2, which lists some data taken from numerical computations for the aerodynamic forces on the three model boomerangs. T_{1x}/F_{1z}, T_{1y}/F_{1z}, T_{1y}/T_{1x} all appear to be increasing with increasing chord, while F_{1z} increases less than proportionally with chord length

bnr	$\dfrac{2c}{2\pi a}$	F_{1z}	$\dfrac{T_{1x}}{F_{1z}}$	$\dfrac{T_{1y}}{F_{1z}}$	$\dfrac{T_{1y}}{T_{1x}}$
244	.00215	.0474	.249	.036	.145
239	.00425	.0809	.264	.057	.219
267	.00645	.1094	.267	.079	.295

Table 32.2. Some aerodynamic data at $\psi = 5°$, U = 1.
c = chord.

In the present section we wish to show the influence of this change in the shape of the lift distribution (due to a change in chord) on a boomerang's flight. Therefore the boomerangs' m and I_3 are chosen in such a way, that *if* the lift distributions were similarly shaped and have magnitudes in the proportion 1:2:3, the resulting flight paths would be identical .In this hypothetical case, the aerodynamic forces, the gravitational forces and the inertial forces all would be in the proportion 1:2:3, provided the boomerangs would be similarly launched.

The flights computed for the three boomerangs have the initial conditions:
$f_o = 10$ rev/s, $V_o = 25$ m/s, $\Psi_o = 0°$,
$\vartheta_o = 70°$, $\varphi_o = 0°$, $\Psi_o = -10°$,
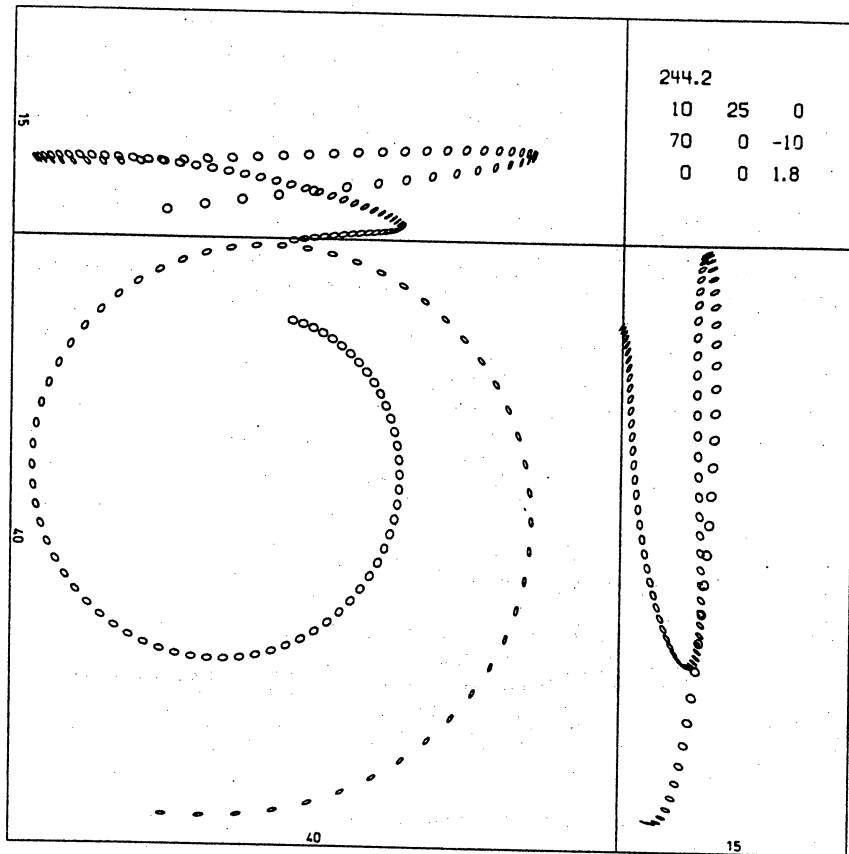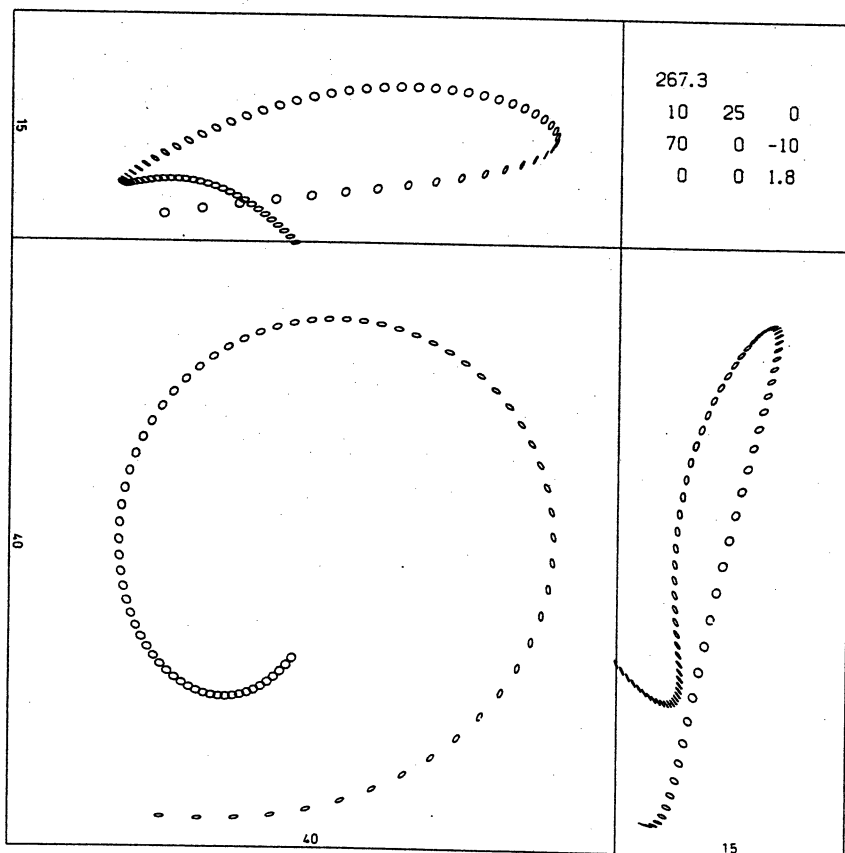$X_o = 0$ m, $Y_o = 0$ m, $Z_o = 1.8$ m,
no wind.

fig. 32.1a

fig. 32.1b

Figure 32.1 shows that the flight paths of the boomerangs 244.2 and 267.3 differ appreciably. The corresponding flight path of boomerang 239.1 is shown in fig. 21.1 b. Some values for the three flights are listed in table 32.3.

bnr	t	P	n	D	Z_2	D_2	D_1	f_2	f_1	V_1	ψ_2	U_1
244.2	9.8	139.0	86.1	33.7	6.0	38.6	10.6	10.0	8.3	7.1	12.9	.41
239.1	8.5	115.1	78.6	22.7	8.2	36.6	9.6	10.0	8.9	8.0	15.2	.45
267.3	8.2	102.8	76.2	13.6	10.3	36.2	8.7	10.0	8.9	5.2	22.0	.29

Table 32.3. Some values of the flights discussed in this section.

The most obvious difference between the three flight paths concerns the maximum elevation (Z_2). Boomerang 244.2 remains very low throughout its flight, but boomerang 267.3 comes considerably higher. This difference can be traced to the differences in the lift distributions mentioned above. The relatively large increase of the pitching torque T_y with increasing chord causes the boomerang with the greatest chord to lie down fastest. Indeed, after flying for one second, the angle ϑ has changed from its initial value $\vartheta_0 = 70°$, to 70.2° for boomerang 244.2, to 66.9° for boomerang 239.1, and to 62.9° for boomerang 267.3.

Both this section and the following one deal with changes in the parameter α_{ot}, which is the geometrical angle of incidence relative to the direction of zero lift, for the profile near the tip of a boomerang arm (see Part II, §22). If a boomerang arm is given a positive twist, its α_{ot} is increased (and the α_{ot} for the reversed profile is decreased, of course). In this section we compare boomerangs having both arms either positively or negatively twisted relative to level 3 boomerang 195.1. Otherwise the boomerangs are the same (see Part II, table 32.1). Table 33.1 lists the respective values of α_{ot} for the three boomerangs considered.

boomerang	arm nr. 1		arm nr. 2	
nr.	normal	reversed	normal	reversed
264.1	+2.0°	+2.0°	-1.0°	+5.0°
195.1	+5.0°	-1.0°	+2.0°	+2.0°
261.1	+8.0°	-4.0°	+5.0°	-1.0°

Table 33.1. α_{ot} for the model boomerangs.

If one would twist both arms of boomerang 195.1 so that the tips would become inclined 3° more upward, one would obtain boomerang 261.1, and if one would apply a negative twist of equal magnitude to the arms of boomerang 195.1, one would obtain boomerang 264.1. It is obvious that for given V, ω_z and $\Psi \geq 0$, boomerang 261.1 experiences more lift, especially near the tips, than boomerang 264.1 does. Some data relevant to the effect of twist on the aerodynamic forces (at $\Psi = 10°$, U = 1) are listed in table 33.2. We see that F_{1z}, T_{1x} and T_{1y} all increase with increasing twist, but T_{1y} increases very little. In particular, the ratio T_{1y}/T_{1x} decreases with increasing twist.

bnr	F_{1z}	T_{1x}	T_{1y}	$\dfrac{T_{1x}}{F_{1z}}$	$\dfrac{T_{1y}}{F_{1z}}$	$\dfrac{T_{1y}}{T_{1x}}$
264.1	.1478	.0315	.0125	.213	.085	.398
195.1	.1644	.0401	.0131	.244	.080	.327
261.1	.1808	.0488	.0138	.270	.076	.282

Table 33.2. Some aerodynamic values at $\Psi = 10°$, U = 1.

Let us now consider the flight paths of these boomerangs, shown in
fig. 33.1a, b, c. They are computed with the initial conditions:

$f_0 = 11$ rev/s, $V_0 = 27$ m/s, $\psi_0 = 0°$,

$\vartheta_0 = 90°$, $\varphi_0 = 0°$, $\psi_0 = -20°$,

$X_0 = 0$ m, $Y_0 = 0$ m, $Z_0 = 1.8$ m,

no wind.

Some values for these flights are listed in table 33.3.

bnr	t	P	n	D	Z_2	D_2	D_1	f_2	f_1	V_1	ψ_2	U_1
264.1	8.4	103.0	74.5	18.6	16.2	44.0	18.5	11.0	7.9	2.0	38.6	.11
195.1	10.2	92.3	99.1	12.9	9.4	22.3	1.2	11.0	9.4	1.7	85.7	.09
261.1	5.5	60.8	52.6	2.2	6.1	15.0	1.8	11.0	8.5	4.2	18.6	.25

Table 33.3. Some values for the flights of fig. 33.1.

The three flight paths have widely different sizes (Z_2, D_2).
Obviously, a twist of 3° can dramatically alter a boomerang's flight
path. Table 33.4 lists some values at t = 1 sec. At this instant the
angle ψ is highest for boomerang 261.1 and lowest for boomerang 264.1,
which is in accordance with the difference in flight path curvature
for these boomerangs. From fig. 33.1 boomerang 264.1 appears to lie
down faster than boomerang 261.1. This is confirmed by table 33.4:
after 1 sec, ϑ has varied relatively fast, and φ relatively slowly
for boomerang 264.1.

bnr	t	f	V	U	ψ	ϑ	φ	ψ
	sec	rev/s	m/s		degr	degr	degr	degr
all	0	11.0	27.0	1.31	0.0	90.0	0.0	-20.0
264.1	1.0	9.0	22.6	1.35	1.8	71.8	39.2	- 3.8
195.1	1.0	10.3	19.1	0.99	10.8	77.5	113.1	-12.8
261.1	1.0	10.6	13.7	0.69	13.4	84.2	155.8	- 1.1

Table 33.4. Some values for the flights at t = 1 sec.

The data presented in this section indicate that even a slight amount
of twist in a boomerang's arms may have a significant effect on the
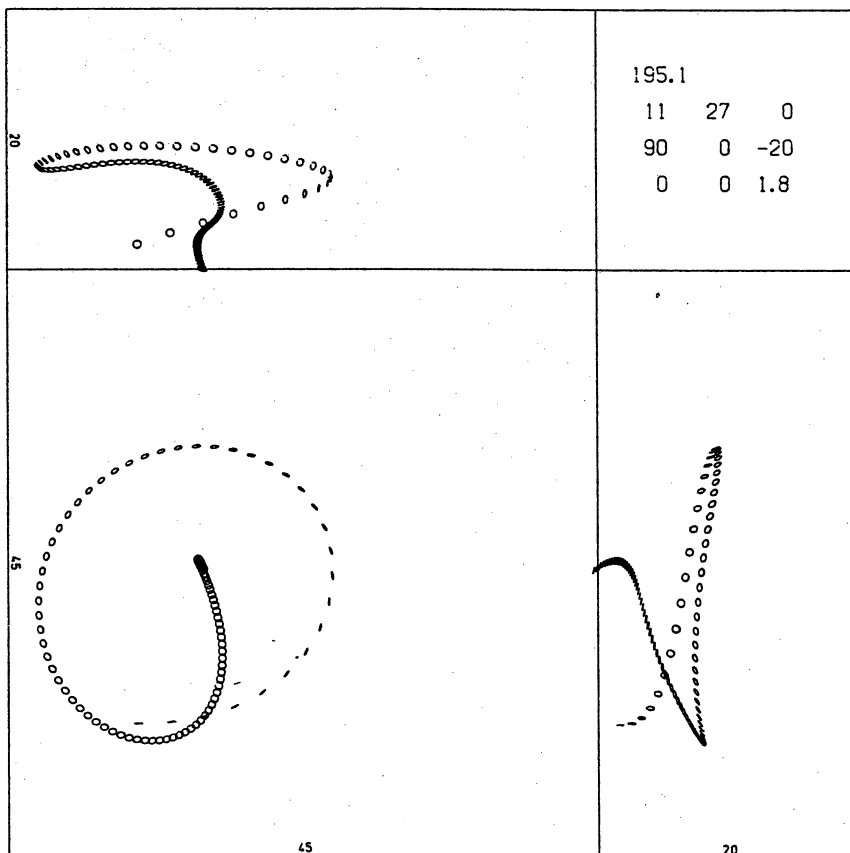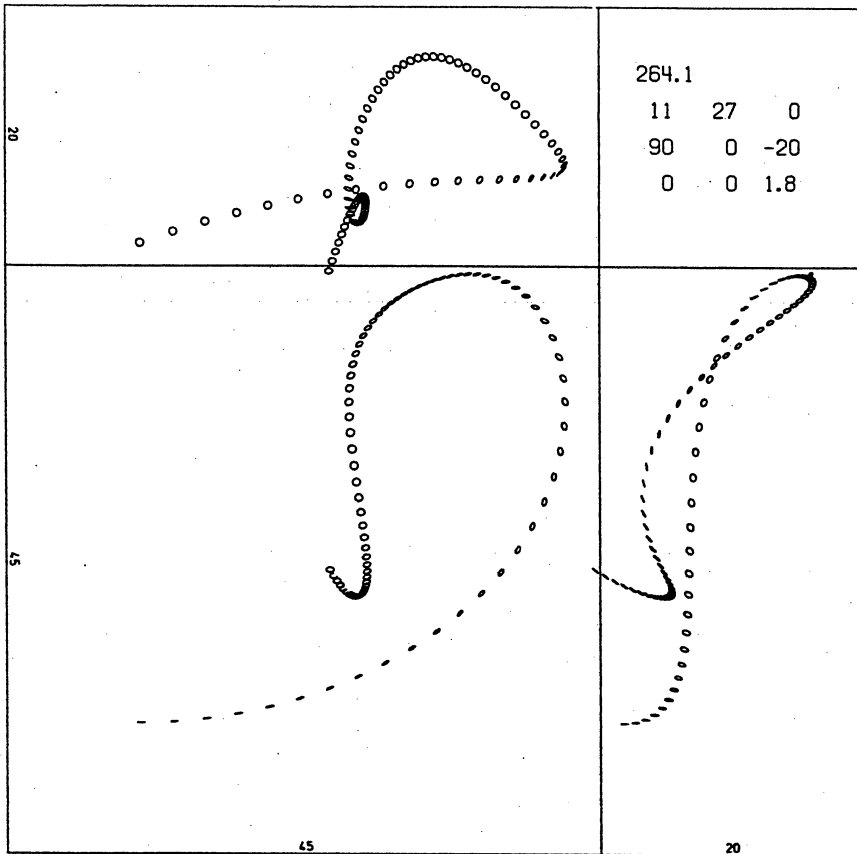flight path.

195.1

11	27	0
90	0	-20
0	0	1.8

fig. 33.1a

264.1

11	27	0
90	0	-20
0	0	1.8

fig. 33.1b

261.1

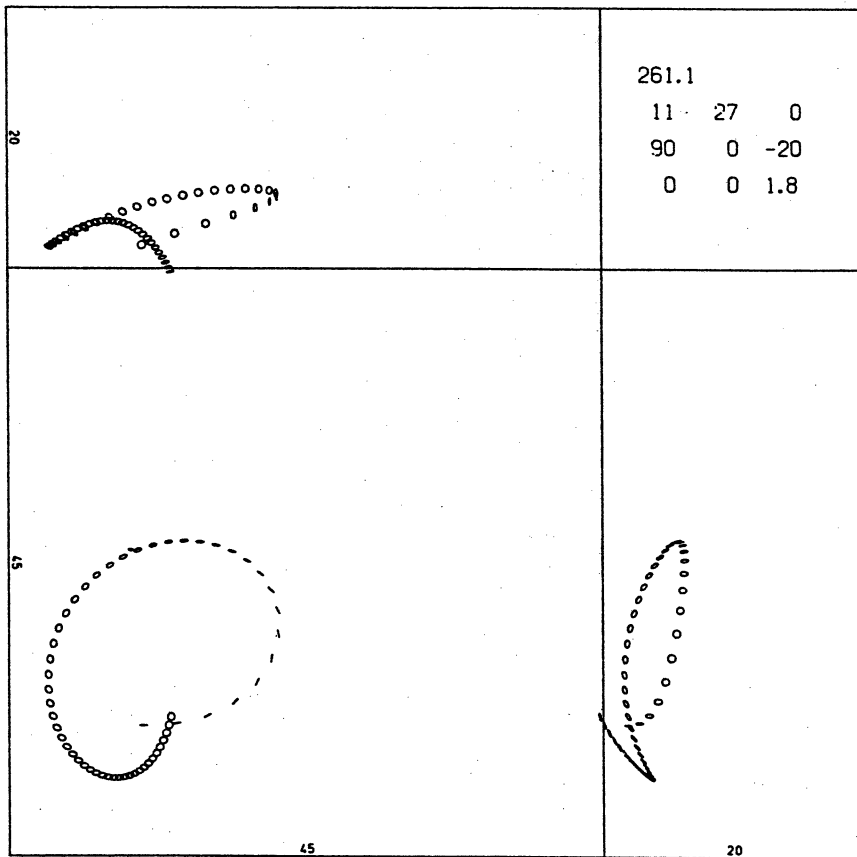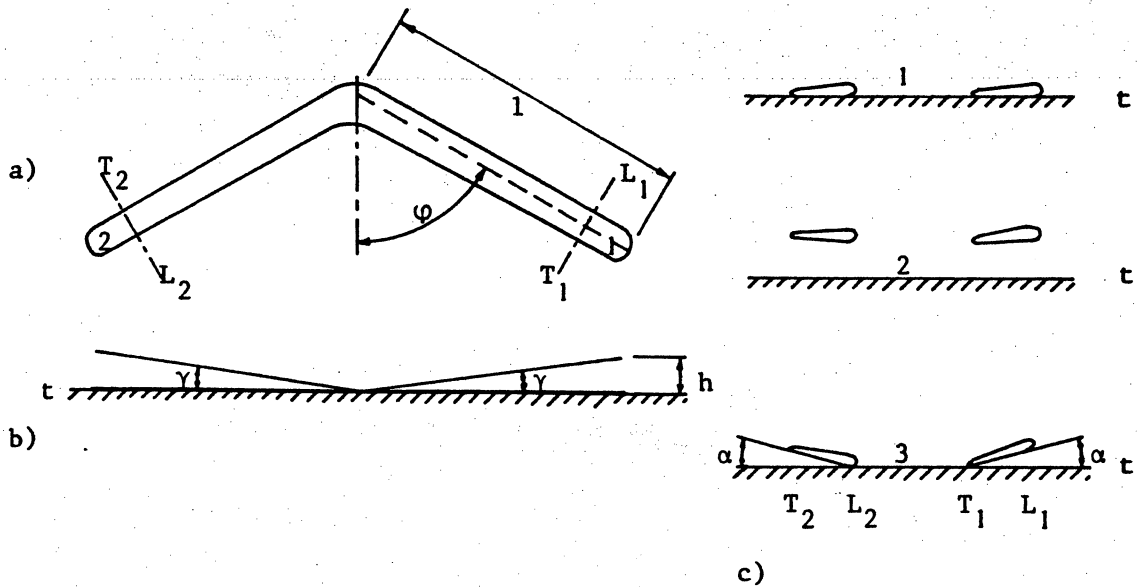| 11 | 27 | 0 |
| 90 | 0 | -20 |
| 0 | 0 | 1.8 |

fig. 33.1c

538

fig. 34.1. Dihedral γ obtained by kinking a plane boomerang at its elbow.
a) Planform of original boomerang resting on a table. 1 = length of arms,
CM = centre of mass, L_1, L_2 = leading edges, T_1, T_2 = trailing edges.
b) Edge-on view, showing dihedral γ. Wing tips are raised at a height h
above the table.
c) Cross sections $L_1 T_1$ and $L_2 T_2$, t = table. 1 : Original position, 2 :
After kinking, raised above the table, 3 : Kinked boomerang resting on
table again.

Let us consider an idealized example (see fig. 34.1). Suppose a boom-
erang rests on a flat table. The boomerang is nearly plane, has a sym-
metrical planform, and consists of two straight, narrow arms of length l,
which include an angle 2φ. The arms are connected by a hinge at the
boomerang's elbow, so that they can rotate with respect to each other
about the line at which the boomerang's plane of symmetry intersects
the table. If the hinge in the elbow is kept in position on the table
and each arm rotates upward over an angle γ, the tips of the arms will
be raised by a distance h = lsinφsinγ above the table. If the hinge is

fixed, with epoxy say, in this position, we have obtained a boomerang with a dihedral angle γ. Note that the boomerang's centre of mass is also raised above the table and that the boomerang's principal axis of inertia is not perpendicular to the table anymore. However, let go of the hinge, and our new boomerang will rest on the table with the trailing edge of its arm nr. 1 (T_1) and the leading edge of its arm nr. 2 (L_2) touching the table. Note that, in this position, the boomerang's main axis of inertia is perpendicular to the table again. The leading edge of arm nr. 1 (L_1) and the trailing edge of arm nr. 2 (T_1) are raised above the table. This means that our new boomerang differs from the original one by a change in the geometrical angle of incidence of its arms. For arm nr. 1 this angle is increased by α, for arm nr. 2 it is decreased by α. The relation between α and γ is given by:

$$\sin\gamma = \sin\alpha \, \cos\varphi \qquad\qquad (34.1)$$

For example, if γ and α are small angles, and the boomerang's arms include an angle $2\varphi = 90°$, we have $\gamma \approx 0.7\alpha$ and $\alpha \approx 1.4\gamma$. For $2\varphi = 120°$: $\gamma \approx 0.5\alpha$, $\alpha \approx 2\gamma$.
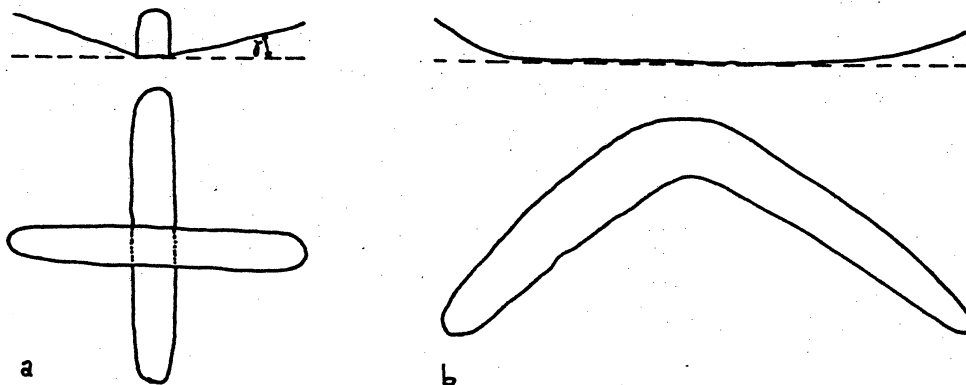

fig. 34.2 a) Cross boomerang with dihedral γ.
         b) Boomerang with wing tips bent upward.

This exposition shows that a two-armed boomerang having a clear-cut dihedral behaves as a boomerang without dihedral, but having arms with changed angles of incidence. However, a cross-boomerang, whose arms are rotated upward over an angle γ, is a quite different case (see fig. 34.2a). The above line of reasoning does not apply to boomerangs with arms whose local spanwise directions deviate from the boomerang's plane

of rotation (= plane perpendicular to principal axis of inertia). Although we did not make calculations for model boomerangs of this kind, such cases can be very well dealt with in our winglet model (see Part II, §2). In the practice of boomerang making it may be interesting to employ the upward or downward bending of the wing tips as one of the factors in the design (see fig. 34.2b). On the other hand, such deformations may be undesirable when they are caused by accidental warp. The upward bend of the tips will nearly always result in (at least a slight) change of the boomerang arms' angles of incidence, as discussed above. However, apart from this effect, it is plausible that the lift on each arm is increased when the arm points forward in the boomerang's flight, and decreased when the arm points backward. This would result in a higher value for the pitching torque T_y, which in turn would cause the boomerang to lie down faster by precession.

Strictly speaking, the model boomerangs for which flight paths are shown in fig. 34.3 do not have a dihedral. The parameter varied is α_{ot}, the geometrical angle of incidence of the profile near the tip of a boomerang arm. If α_{ot} is increased for one arm, it is decreased by the same amount for the other arm. The corresponding angle at the root of the arm, α_{or}, is kept constant. (For a definition of these parameters, see Part II, §22.) The model boomerangs differ from each other only in α_{ot}, otherwise they are identical with boomerang 195.1 (see Part II, table 32.1). Values of α_{ot} for the three boomerangs considered are listed in table 34.1. Roughly speaking, if boomerang 195.1 is given a positive dihedral of about 2°, one would obtain a boomerang more or less resembling the 262.1, and if boomerang 195.1 is given a negative dihedral of about 2°, one would obtain a boomerang more or less resembling the 263.1. Strictly speaking, one obtains boomerang 262.1 from boomerang 295.1 by giving arm nr. 1 a positive twist of 3°, and arm nr. 2 a negative twist of 3°. For boomerang 263.1 the converse is true.

The effect of the chosen variations in α_{ot} on the aerodynamic forces are illustrated by table 34.2, which lists some data for $\Psi = 10°$, $U = 1$. *Only T_{1y} varies, the five other components* (including those not listed here) *remain essentially constant.* This remarkable phenomenon can be observed in many other computed cases, in which the angle of incidence

boomerang	arm nr. 1		arm nr. 2	
nr.	normal	reversed	normal	reversed
263.1	+2.0°	+2.0°	+5.0°	−1.0°
195.1	+5.0°	−1.0°	+2.0°	+2.0°
262.1	+8.0°	−4.0°	−1.0°	+5.0°

Table 34.1. α_{ot} for the model boomerangs.

is increased for one arm and decreased by the same amount for the other arm. The net result of such a modification appears to be a shift of a part of the average lift forward or backward over a distance proportional to the difference in excentricity of the boomerang arms concerned. The magnitude of this effect can also be calculated by means of the simple model of [Hess, 1968], in which the induced velocity of the air is neglected. It is remarkable that the results of this model closely agree with those of the winglet model. For an explanation of the effect see [Hess, 1968, p. 131] and also Part I, §17. (Excentricity: Part II,§ 20).

bnr	F_{1z}	T_{1x}	T_{1y}	$\dfrac{T_{1x}}{F_{1z}}$	$\dfrac{T_{1y}}{F_{1z}}$	$\dfrac{T_{1y}}{T_{1x}}$
263.1	.1660	.0404	.0102	.244	.061	.252
195.1	.1644	.0401	.0131	.244	.080	.327
262.1	.1622	.0399	.0161	.246	.099	.403

Table 34.2. Some aerodynamic values at $\Psi = 10°$, $U = 1$.

Figure 34.3a,b and fig. 33.1a show flight paths computed for the three boomerangs with the following initial conditions:

$f_o = 11$ rev/s, $V_o = 27$ m/s, $\Psi_o = 0°$,

$\vartheta_o = 90°$, $\varphi_o = 0°$, $\psi_o = -20°$,

$X_o = 0$ m, $Y_o = 0$ m, $Z_o = 1.8$ m,

no wind

Some values for these flights are listed in table 34.3.

Obviously, a main difference between the three flight paths concerns the maximum elevation (Z_2). Boomerang 263.1 remains relatively low, whereas boomerang 262.1 attains a considerably greater height. This was
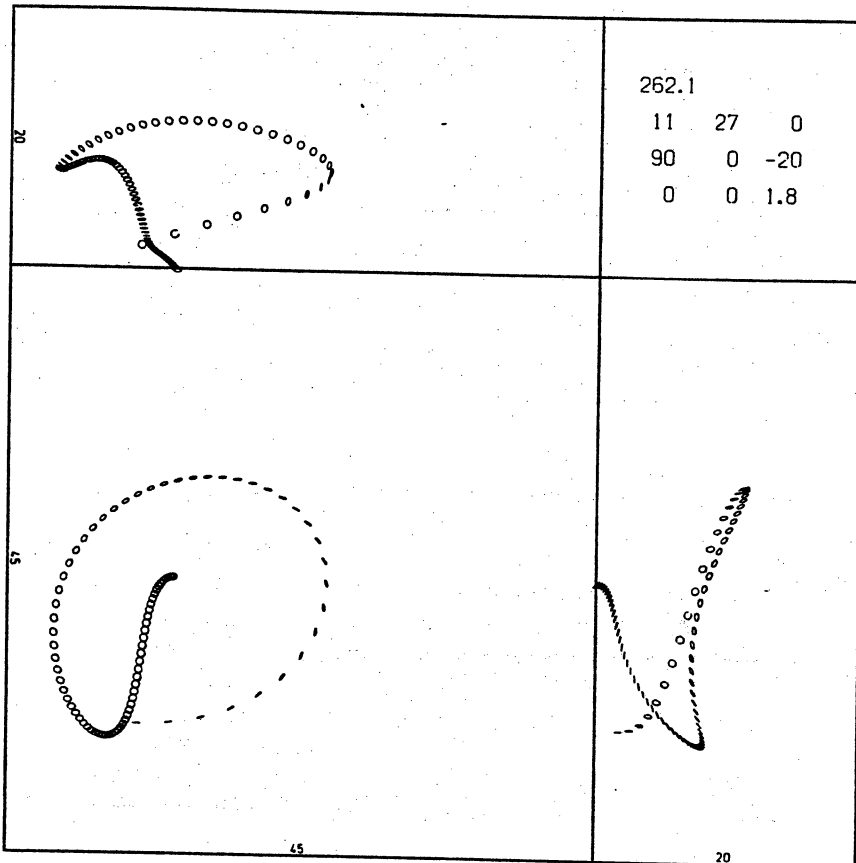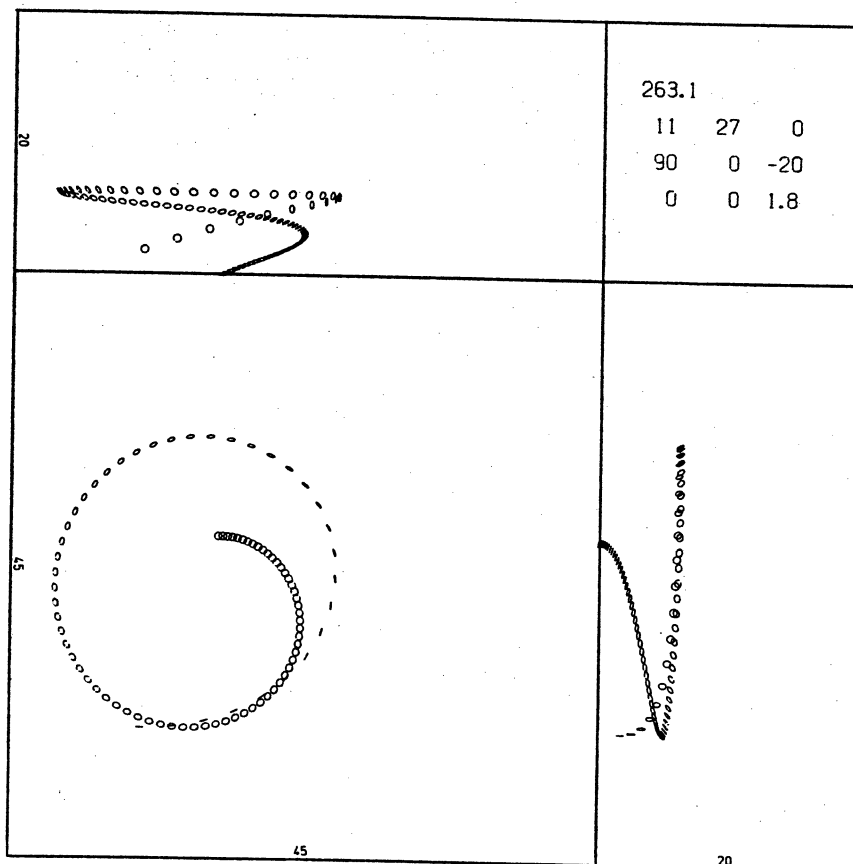
262.1
11   27   0
90   0   -20
 0   0   1.8

fig. 34.3a

263.1
11   27   0
90   0   -20
 0   0   1.8

fig. 34.3b

bnr	t	P	n	D	Z_2	D_2	D_1	f_2	f_1	V_1	Ψ_2	U_1
263.1	8.8	97.0	86.1	16.0	6.3	23.3	0.8	11.0	9.4	3.9	29.2	.22
195.1	10.2	92.3	99.1	12.9	9.4	22.3	1.2	11.0	9.4	1.7	85.7	.09
262.1	8.6	80.9	78.1	11.6	11.4	20.7	0.9	11.0	8.5	2.8	43.9	.17

Table 34.3. Some values of the flights of fig. 34.3 and fig. 33.1a.

to be expected on the basis of the differences in the torque T_y: boomerang 262.1 lies down faster than boomerang 263.1 does. Table 34.4 lists some values at $t = 1$ sec.

bnr	t	f	V	U	Ψ	ϑ	φ	ψ
	sec	rev/s	m/s		degr	degr	degr	degr
all	0	11.0	27.0	1.31	0.0	90.0	0.0	-20.0
263.1	1.0	10.3	20.0	1.04	9.6	80.1	108.2	- 3.6
195.1	1.0	10.3	19.1	0.99	10.8	77.5	113.1	-12.8
262.1	1.0	9.9	17.7	0.95	13.2	77.4	121.0	-22.2

Table 34.4. Some values for the flights at $t = 1$ sec.

A qualitatively similar influence of variations in T_y on the shape of boomerang flight paths was shown in [Hess, 1968, p. 134] (there the parameter β equals $arctg(T_{1y}/T_{1x})$).

A boomerang which traverses a curved path shaped like a quarter circle and which cannot be thrown to return properly, might be called a non-returning boomerang. Straight-flying boomerangs, however, are subtle instruments, at least as specialized as good returning boomerangs. By far the best report on this type of boomerang is that by Mr. Errett Callahan [1975]:

All afternoon we threw back and forth, up and down the meadow. Robert [Gillum], of huge stature, got flights of up to 190 yds [175 m]. My best was 170 [155 m]. The boomerang was so finely tuned that, with proper release, we were able to obtain virtually straight-line flights with no noticeable deviation to left or right. We threw the N.R.B. [non-returning boomerang] with the limbs parallel to the ground (maybe tilted up as much as 5°). The flights stayed a constant 3 ft. [1 m] or so above the ground till near the very end, flying in a most spectacular bee-line, rotating like a propeller all the way. The distances we threw that day remain our best to date. Yet we feel that a slightly heavier N.R.B. would have given us throws of over 200 yds [180 m]. The piece we used was of the following specifications: sourwood (Oxydendrum arboreum), L [tip-to-tip length] = 26" (66.2 cm), W [width of limbs] = 2¼" (5.7 cm), T [thickness] = 3/8" av. (1 cm), C [circumference of profile] = 4¾" av. (12.1 cm), X [shape of profile] = lenticular, Wt [weight] = 7 oz. (200 g), $\angle$ B [angle included between limbs] = 136°, %R [=100 L/R] = 153, R [radius of curvature] = 17" [43 cm].   [Callahan, 1975, p.35]

I have not experimented with straight flying boomerangs myself, but instead tried to design a theoretical model boomerang capable of flying long distances along an approximately straight, horizontal path. The principle of the straight-flying boomerang is mentioned in Part I, §17 (see also [Musgrove 1974]). Occasional returning boomerangs, when thrown with opposite spin at $\vartheta \approx 0$, traverse nearly straight horizontal flight paths.

The model boomerang discussed below is derived from boomerang 195.1 (which is associated with the experimental boomerang L1 (see table 10.1.) by giving both arms a negative twist, and increasing the mass and the moment of inertia. Table 35.1 contains the aerodynamic input parameters for boomerang 215.5. Additional parameters are:
a = .298 m, m = .200 kg, I_3 = .00600 kg m^2, λ = .338.

arm	e	l	c_t	c_r	α_{ot}	α_{or}	dC_L	C_{L1}	C_{L2}	C_{L3}	C_{L4}	C_{Dm}	dC_D
1	+71	286	43	57	-5.0	+6.0	.10	-1.0	+1.6	-0.5	+1.0	.06	.03
	reversed profile				+9.0	+6.0	.10	-1.0	+2.4	-0.5	+1.0	.08	.03
2	-61	296	41	57	-1.0	+6.0	.10	-1.0	+1.6	-0.5	+1.0	.06	.03
	reversed profile				+5.0	+6.0	.10	-1.0	+2.4	-0.5	+1.0	.08	.03

Table 35.1. Parameters characterizing aerodynamic properties of boomerang 215. Lengths in mm, angles in degrees. Symbols explained in Part II, § 22.

To sum up the differences between boomerang 215.5 and boomerang 195.1 (or 195.2): (I) The negative twist of the arms; for arm nr. 1 α_{ot} is decreased by $10°$, for arm nr. 2 by $3°$. For both arms α_{or} is decreased by $2°$. (II) $C_{L2} = 1.6$ instead of 2.0. However, almost the same flight paths were computed for a boomerang (213.5) with $C_{L2} = 2.0$, but otherwise identical with boomerang 215.5. (III) C_{L4} for the reversed profiles is 1.0 instead of 0.8. This difference is unimportant. (IV) Boomerang 215.5 is more massive than boomerangs 195.1 and 195.2, and its value of $\lambda = I_3/ma^2$ is higher.

The two flight paths shown in fig. 35.1a and b have the following initial conditions:

case A: $f_o = 10$ rev/s, $V_o = 25$ m/s, $\Psi_o = 5°$,
$\vartheta_o = 25°$, $\varphi_o = 5°$, $\Psi_o = -15°$,
$X_o = 0$ m, $Y_o = 0$ m, $Z_o = 1.5$ m,
no wind.

case B: $f_o = 10$ rev/s, $V_o = 25$ m/s, $\Psi_o = 5°$,
$\vartheta_o = 10°$, $\varphi_o = 15°$, $\Psi_o = -15°$,
$X_o = 0$ m, $Y_o = 0$ m, $Z_o = 1.5$ m,
no wind.

The difference in flight path shape between the cases A and B is exclusively due to the difference in ϑ_o. In both cases $\Psi_o = 5°$. Trials with $\Psi_o = 0°$ or $10°$ resulted in substantially shorter flight paths. This indicates that, for boomerang 215.5, the path length may be very sensitive to the initial conditions, which would be undesirable in the practice of boomerang throwing. Some values for flights A and B are
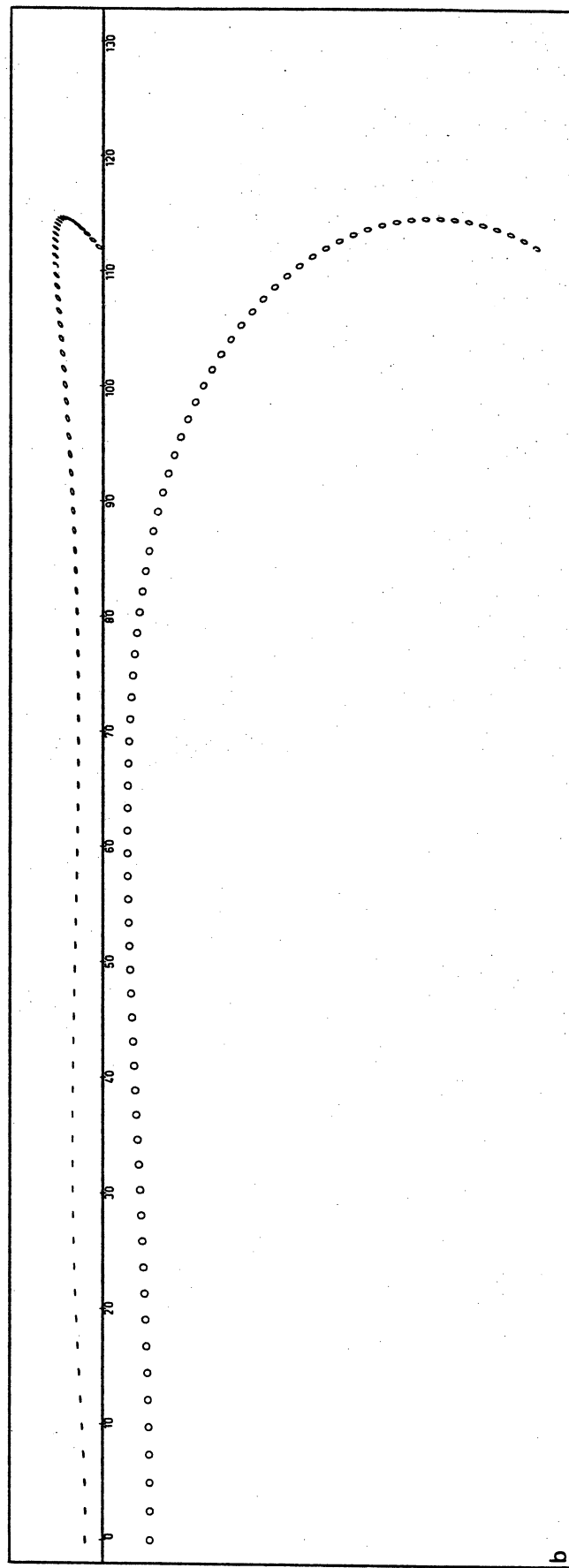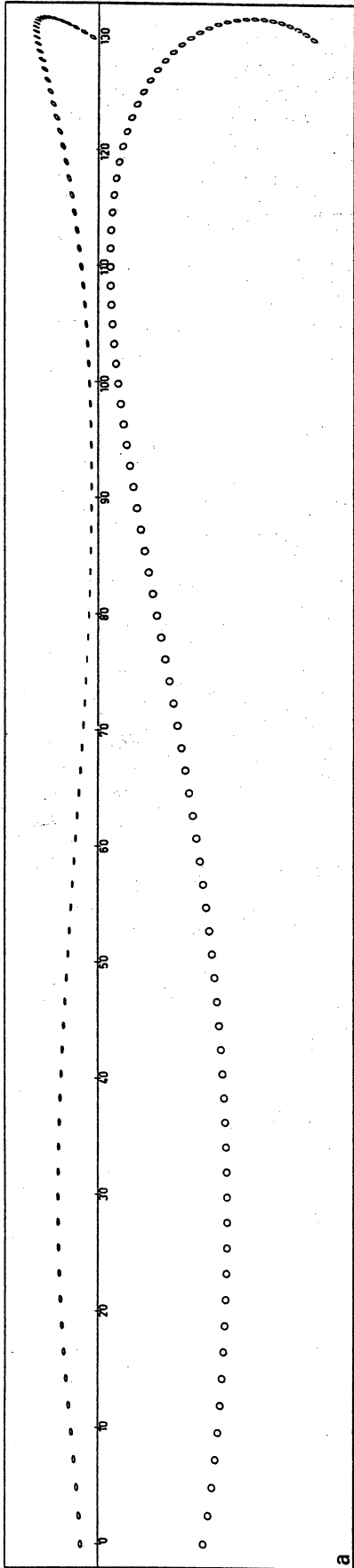
fig. 35.1. Two flight paths of boomerang 215.5, side view and bird's-eye view. a) case A, b) case B.

listed in table 35.2.

	t	P	n	D	Z_2	D_2	D_1	f_2	f_1	V_1	Ψ_2	U_1
A	8.7	147.3	60.6	129.9	5.4	131.9	129.9	10.0	5.7	8.4	19.2	0.70
B	7.7	138.1	54.4	116.5	4.1	117.5	116.5	10.0	5.9	12.7	10.9	1.13

Table 35.2. Some values for the flights of fig. 35.1.

During the greater part of both flights the angle of incidence Ψ remains very small. In fact: $0° < \Psi \leq 5°$ up to t = 5.0 sec, P = 103 m in case A, and up to t = 4.4 sec, P = 91 m in case B. Figure 35.2 shows (Ψ, U)-diagrams for both cases. Some values relating to the instant at which a path length of 100 m is reached can be found in table 35.3. This distance is covered in about 5 seconds, hence the boomerang's average speed over this trajectory is 20 m/s (72 km/h). After travelling 100 metres, the boomerang's initial kinetic energy of 74.3 J is diminished to 47% in case A and to 40% in case B.
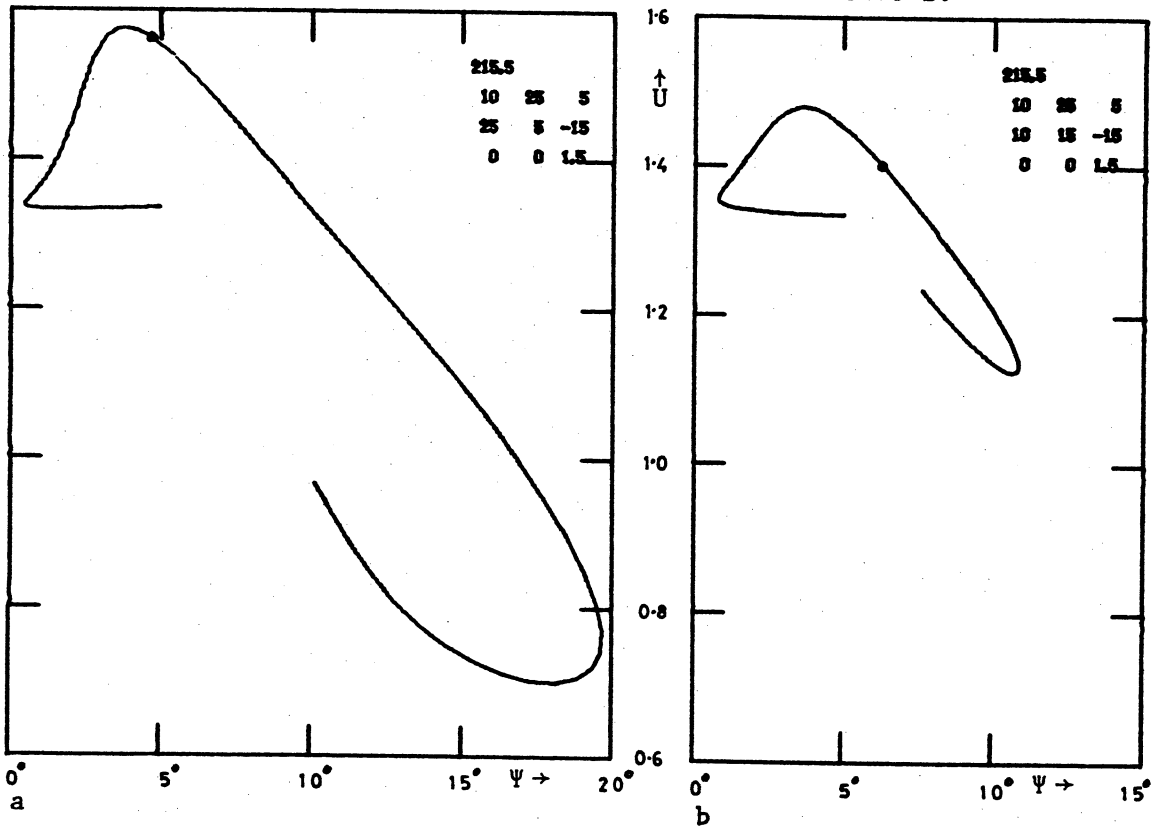
Fig. 35.2. (Ψ, U)-diagrams. a: case A, b: case B.
A dot indicates the instant at which P = 100 m.

	t	f	V	U	ψ	θ	E
	sec.	rev/s	m/s		degr	degr	J
A	4.9	6.0	17.7	1.56	4.7	13.5	35.1
B	5.0	6.1	15.9	1.40	6.4	34.0	29.7

Table 35.3. Some values at the instant t for which P = 100 m. E is kinetic energy in Joules.

The performance of a wing at low Reynolds numbers (Re $\lesssim 10^5$) may be improved by the attachment of a wire in front of the profile's nose, parallel to the wing's leading edge (see [Schmitz, 1954]). Such a turbulence wire helps the boundary layer to become turbulent, and lowers the critical Reynolds number. The airflow around the wing becomes supercritical more easily, which may result in a higher lift and a smaller drag. A similar effect may occur when a wing's round nose is sharpened. If the turbulence wire touches the wing's surface, it can be called a trip wire [Kraemer, 1961]. The effect of a turbulence wire on the lift and drag of a wing in a straight airflow is also reported in Part II, §26. However, as is discussed in Part II, §33, this effect may be rather different for rotating boomerangs, where the rotation by itself appears to lower the local critical Reynolds number of the boomerang arms.

We have tried to investigate this matter by doing various – albeit not very systematic – field experiments. The following methods were used to influence the boundary layer of the airflow around the boomerang arms:

A) Application of trip wires. Lengths of cotton thread were attached to the boomerang's leading edges by means of adhesive tape applied near the wing tips and near the elbow.

B) Rounding or sharpening the leading edges, by sanding or filing away some material.

C) Smoothing or roughening of the boomerang's surface, by sanding, filing or application of rough adhesive tape.

Most of the boomerangs concerned were visibly influenced in their flying behaviour by the above modifications. However, I could not find systematic trends in the observed effects. Some boomerangs performed much better with trip wires than without, whereas other boomerangs flew poorly with trip wires. Some boomerangs lied down more slowly, and could even traverse two horizontal circles, after their leading edges were made sharper, but other boomerangs only lost their spin more quickly. For some boomerangs the roughness or smoothness of

their surfaces made little difference, others performed best with smooth surfaces. In all cases the condition of the boomerang's underside did not matter much.

One observation indicates that a boomerang's central part, near its elbow, is aerodynamically relevant. Boomerang L4 was thrown with its batteries removed under two conditions: respectively with adhesive tape covering the rectangular hole for the batteries, and without this tape, leaving the hole exposed. Under the latter condition, the boomerang suffered so much air resistance that it flew very poorly indeed.

More systematic experiments are needed, involving the careful design of boomerangs with various profiles, the use of turbulence wires, and the launching of boomerangs at controlled initial conditions.

Figures 36.1 and 36.2 present some photographed flight paths of boomerang L4, both plain and with trip wire. More information on this boomerang can be found in §17. The attachment of trip wires significantly improves the performance of this boomerang. Compare fig. 36.1 a and b with c and d. The initial conditions for these flights may differ somewhat, but qualitatively the influence of the wire is shown quite well. Without wire, the boomerang descends steeply after the first half of its flight. With wire, the boomerang stays higher in the air. Fig. 36.2 a and b present a similar comparison. In fig. 36.2a boomerang L4 plain is badly launched and hits the ground after 4 sec. In fig. 36.2b boomerang L4 with wire is launched in about the same manner, but now the flight path curves up enough for the boomerang, to fly on. Fig. 36.2c shows a roughly similar flight path of the Ly with wire, but here the boomerang is launched in a different direction.
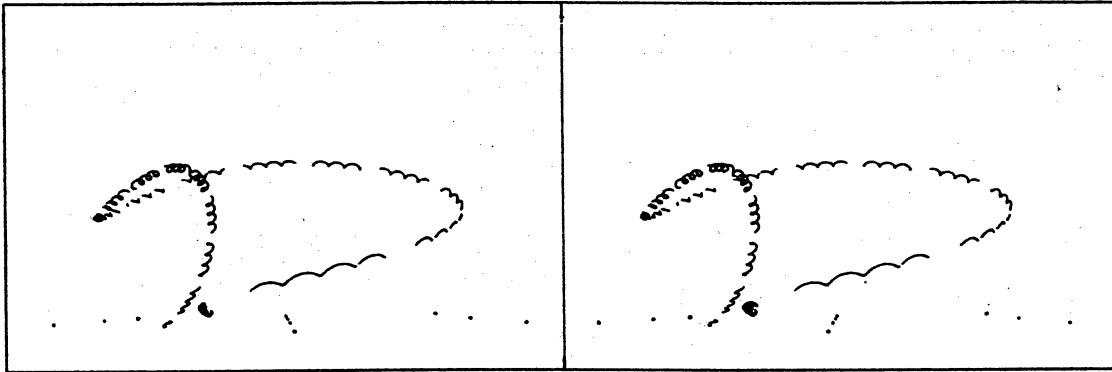
What is the aerodynamic difference between boomerang L4 plain and boomerang L4 with wire? Probably the boomerang with wire flies at a smaller angle of incidence Ψ, traverses a somewhat wider loop, and loses its energy less quickly than the boomerang without wire does. A smaller value of Ψ would indicate that the wire causes a
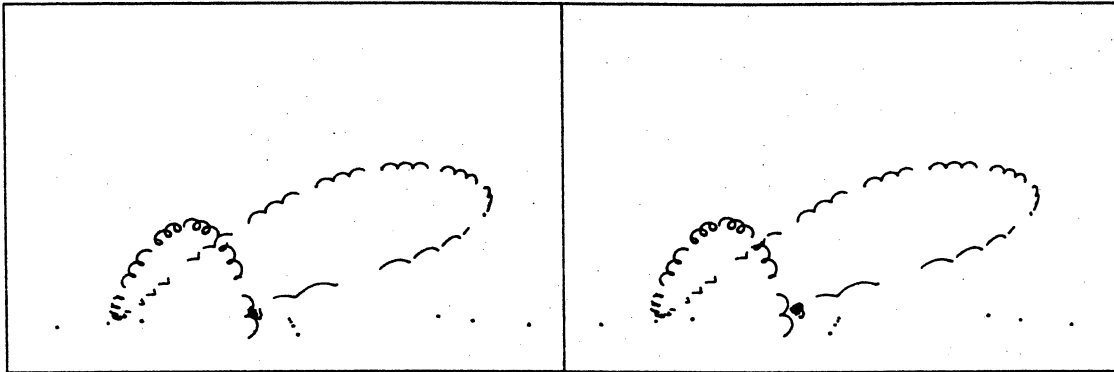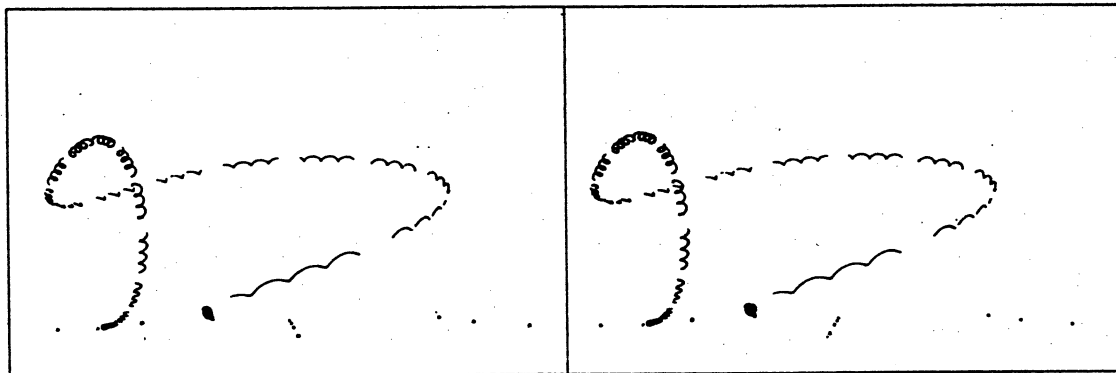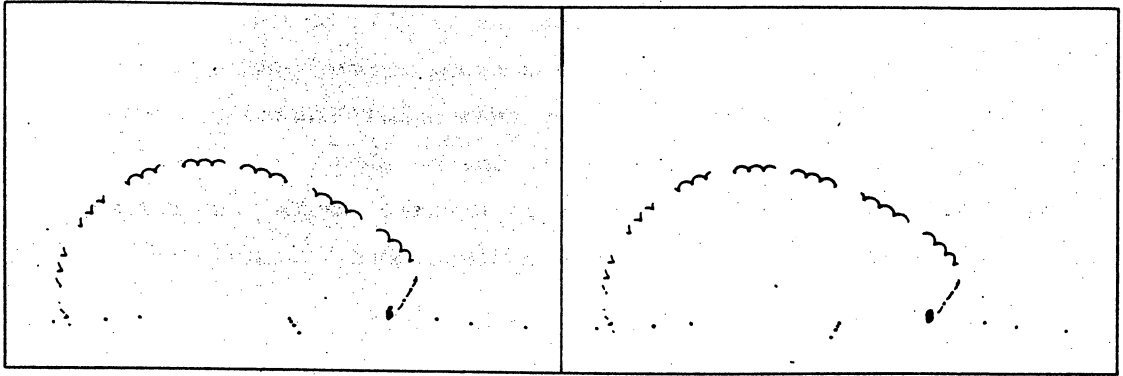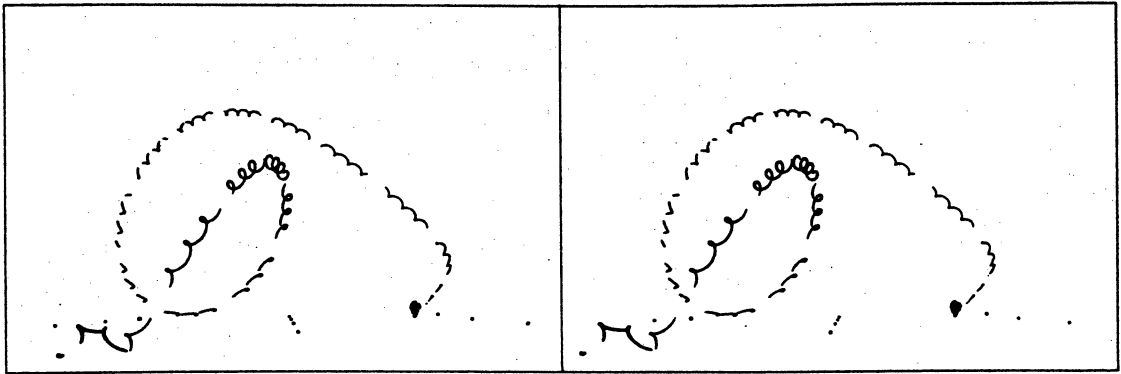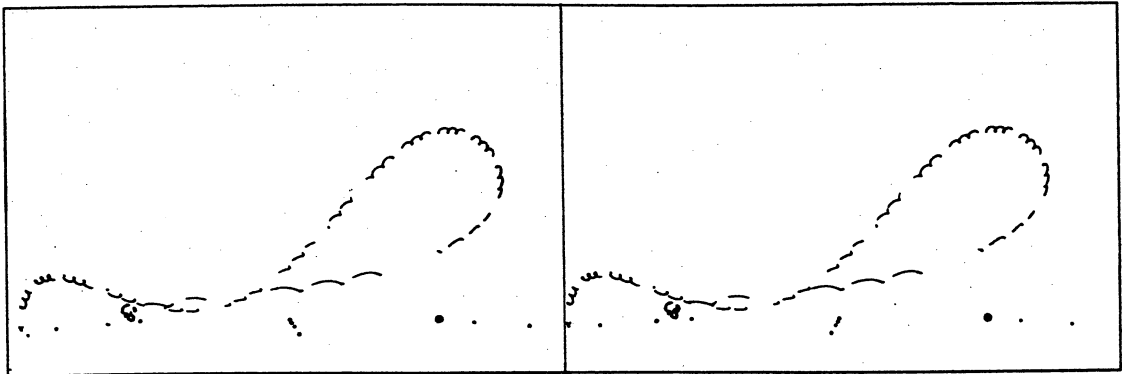
fig. 36.1. a: L4 plain, 14R29A/L29A. b: L4 plain, 14R23A/L23A.
c: L4 with wire, 14R13A/L13A. d: L4 with wire, 14R15A/L15A.

552

fig. 36.2. a: L4 plain, 8R24A/L24.
      b: L4 with wire, 14R18A/L18A.
      c: L4 with wire, 10R6/L4.

decrease in the ratio T_{1x}/F_{1z}. As remarked in §17, we did not succeed in finding a suitable level 3 model boomerang corresponding to the L4 with wire, under the condition that this model boomerang should differ from the 237.1 (corresponding to the L4 plain, see Part II, table 32.1) in only one or two of the aerodynamic input parameters (for instance α_{or} and/or α_{ot} might be changed, and C_{L2} might be higher).

References for Part III

Birkhoff, G., 1950.
Hydrodynamics, a study in logic, fact and similitude. (Princeton Univ.Pr., 1950. reprint Dover Publ., New York, 1955)

Bridgman, P.W., 1931.
Dimensional analysis. (Yale Univ.Pr., New Haven, 1931)

Buchner, M., 1916.
"Das Bumerangwerfen". Zeitschrift für Ethnologie 48 (1916) p. 219-231

Buchner, M., 1918.
Das Bumerangwerfen. Ein wissenschaftlicher Sport. (München, 1918)

Callahan, E., 1975
The non-returning boomerang: evolution and experiment (typescript, Anthro. Dept. Virginia Commonwealth University, Richmond, Va., 1975)

Hanson, M.J., 1974.
The boomerang book (Penguin Books Ltd., England, 1974)

Hauser, W., 1965.
Introduction to the principles of mechanics. (Addison-Wesley, Reading, Mass., 1965)

Hess, F., 1968.
"The aerodynamics of boomerangs". Scientific American, 219, 5 (Nov. 1968) p. 124-136

Hess, F., 1973.
Boomerang dynamics. (Report TW-129, Mathematisch Instituut, Rijksuniversiteit Groningen, 1973)

Jeffery, G., Grantham, A. & Hersey, J., 1973.
The aerodynamics of boomerangs (typescript, Dept of Applied Physicsl Sciences, University of Reading, U.K., 1973)

Kraemer, K., 1961.
"Über die Wirkung von Stolperdrähten auf den Grenzschichtumschlag". Zeitschrift für Flugwissenschaften, 9, 1 (1961) p. 20-27

Musgrove, P.J., 1974.
"Many happy returns." New Scientist 61, 882 (1974) p. 186-189

Pfaundler, L., 1905.
"Über einen Bumerang zu Vorlesungszwecken". Berichten der Wiener Akademie 114, 2A (1905) p. 647-648

Pfaundler, L., 1906.
Müller-Pouillets Lehrbuch der Physik und Meteorologie Bd. 1 (10th ed. Braunschweig, 1906) p. 322-324

Schmitz, F.W., 1954.
"Zur Aerodynamik der kleinen Reynolds-Zahlen." Jahrbuch 1953 Wiss. Ges. Luftfahrt (Braunschweig, 1954) p. 149-166